STUDIES ON LASER ABLATION OF POLYMER COATED PROPELLANT FILMS

Except where reference is made to the work of others, the work described in this thesis is my own or was done in collaboration with my advisory committee. This thesis does not include proprietary or classified information.

_____
Artem Dyachenko

Certificate of Approval:

| | |
|---|---|
| German Mills | Rik Blumenthal, Chair |
| Associate Professor | Associate Professor |
| Chemistry and Biochemistry | Chemistry and Biochemistry |

| | |
|---|---|
| Andreas J. Illies | Stephen L. McFarland |
| Professor | Acting Dean |
| Chemistry and Biochemistry | Graduate School |

STUDIES ON LASER ABLATION OF POLYMER COATED PROPELLANT FILMS

Artem Dyachenko

A Thesis

Submitted to

The Graduate Faculty of

Auburn University

in Partial Fulfillment of the

Requirements for the

Degree of

Master of Science

Auburn, Alabama
August 7, 2006

STUDIES ON LASER ABLATION OF POLYMER COATED PROPELLANT FILMS


Artem Dyachenko

_____
Signature of Author


_____
Date of Graduation

VITA


Artem Aleksandrovich Dyachenko, son of Alexander and Elena, was born in Moscow, Russia on December 22, 1979. Upon graduation from High School in June, 1996, he entered the Physical Chemistry Department at Russian University of Chemical Technology where he graduated from in March, 2003 with a Bachelor of Science degree in Chemical Engineering. Artem began his graduate studies at Auburn University, Auburn, Alabama in August, 2003.

THESIS ABSTRACT

STUDIES ON LASER ABLATION OF POLYMER COATED PROPELLANT FILMS

Artem Dyachenko

Master of Science, August 7, 2006
(B.S., Russian University of Chemical Technology, 2003)

69 Typed Pages

Directed by Rik Blumenthal

In artillery, safety issues make propellants highly preferable as compared to ordinary explosives. However, the same properties that make propellants safer, such as their low shock sensitivities, also make them more difficult to ignite directly. In large bore artillery shells, ignition of the propellant is achieved using a small amount of an ordinary explosive, such as lead azide, as the primer. This sequential ignition process results in irreproducible delays that prevent targeting of fast moving objects. Numerous attempts have been made to develop improved ignition processes. Laser ignition would overcome the ignition delay problem and be practical. Unfortunately, all of the propellants used today cleanly ablate under laser irradiation, and ignition cannot be

achieved. Electrothermal Chemical (ETC) ignition has proved capable of overcoming the ignition delay problem, but it is not practical. In this method, a large capacitor is discharged across a small piece of plastic, generating a high-pressure, high-temperature plasma that ignites the propellant after a short and highly reproducible delay. Unfortunately, the capacitor and related power supply to charge it are too large and heavy for practical application of ETC ignition. In this work, a new approach to ignition is developed based on the generation of a high-temperature, high-pressure plasma, directly at the propellant surface, that has a chemical composition similar to that of the ETC igniter, using laser ablation of the plastic coating on the propellant.

ACKNOWLEDGMENTS

Style manual or journal used: American Chemical Society style

Computer software used: MS Word 2003, MS Excel 2003, Adobe Photoshop CS2

TABLE OF CONTENTS

# LIST OF FIGURES

# I. INTRODUCTION

## I.1 PROPELLANTS

A propellant is defined as a rapid burning charge that propels a bullet, shell, rocket, or missile.[1] Unlike primary explosives, propellants are temperature and pressure dependent and therefore require the use of detonator and also possibly a booster. A detonator contains a primary explosive as an essential element; however, it may be more complex. This is true particularly of military detonators, or fuses and delay blasting caps in which timing, safety, and other mechanisms are also built into the detonator. A booster is a sensitive secondary explosive which reinforces the detonation wave from the primary explosive, or detonator, and delivers thereby a more powerful detonation wave to the main (secondary) explosive charge. Examples of primary explosives include lead azide, mercury fulminate and nitromannite. Primary explosives are very sensitive to heat, impact or friction and detonate or burn very rapidly. Nearly all combustible gases and dusts can be explosive when mixed with air in certain proportions, e.g.:

$$CH_4 + 2O_2 \rightarrow CO_2 + 2H_2O + heat \qquad (1)$$
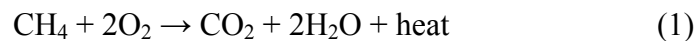
Many gaseous and dust-air or dust oxygen explosives are, in fact, primary explosives, since they are readily detonated in a manner characteristic of primary explosives, frequently with exceedingly small sources of energy. For this reason, combustible gases and dusts are extremely dangerous explosion hazards and have been responsible for

numerous residential and industrial accidents and fatalities. Primaries often need $O_2$ gas as a reactive. Grain dust such as lycopodium powder is not especially flammable but when grain is dumped into a grain silo, some of the finer dust particles can remain suspended in air surrounded by oxygen. This mixture can be ignited by a spark, resulting in an explosion. Primary explosives, detonate when initiated, but they are extremely sensitive and, as a class, have less power than secondary explosives such as TNT, RDX and HMX which have the highest energy outputs of any explosives.[2, 3] The energy output is proportional to the volume of the gaseous products of explosion, e.g. during detonation of RDX, a relatively large number of net gas molecules formed:

$$C_3H_6O_6N_6 \rightarrow 3CH_2N + 3NO_2 \qquad (2)$$
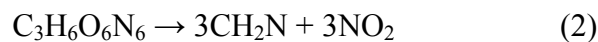
Propellants have a number of advantages over primary explosives. They are less sensitive to heat and shock than primary explosives: most simply burn rather than explode when ignited in air, and can be detonated only by the nearby explosion of a primary initiator. Two common propellants used by the Army are RDX (Research Department Explosive) and HMX (High Melting Explosive), see Figure 1.1.
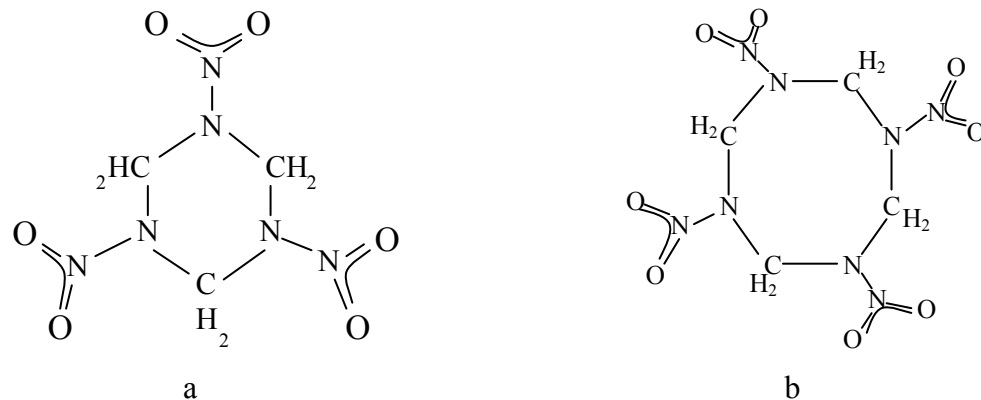


Figure 1.1 – a) RDX molecule; b) HMX molecule

2

Propellants are used by military as fillings for bombs and shells with only a small amount of primary explosive needed. This makes the explosive devices safer and less susceptible to accidental explosions. The initiation of secondary explosives generally requires the shock wave energy from a primary explosive. Secondary explosives will not detonate when subjected to a spark, flame, or a hot wire as will a primary explosive.

I.2 IGNITION TECHNIQUES

Conventional ignition requires the use of primary explosive such as a military fuse to initiate the explosion of a less sensitive secondary explosive. The simplest fuse is a length of combustible material which burns from the free end, through a small opening in the casing, into the explosive charge, where it then ignites the explosive material, see Figure 1.2. A typical large bore shell contains an ordinary fuse cap, primary and secondary explosives. The black powder in an ordinary fuse cap refers to a low explosive such as sodium nitrate, sulfur or charcoal and serves as a safety fuse.

Primary Explosive
$((Pb(N_3)_2)$

Fuse with Black Powder Core
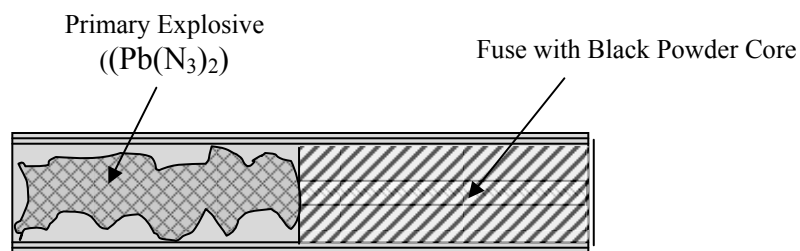
Figure 1.2 - Ordinary fuse cap.

3

In the ordinary fuse cap, a primary explosive such as lead azide is used alone to fulfill the threefold primary purposes of the cap: ignition of pre-detonation explosion, creation of the detonation wave, and delivery of sufficiently intense detonation wave to a secondary charge to detonate this main charge.[2] Lead from the primary explosive is released in the barrel of the gun and then deposits on the interior of the barrel and must be removed later as it builds up. Lead also is released into the air where it may result in a hazardous exposure to the troops operating the gun. One motivation to replace conventional ignition is the elimination of lead.

A typical primary explosive used in the Army is environmentally hazardous lead azide ($Pb(N_3)_2$) which can be avoided by using plasma ignition technique. The interest of this research is the process of plasma ignition which removes the need for lead azide completely. In plasma ignition systems, also referred to as electrothermal chemical (ETC) ignition, an ordinary fuse cap is replaced by a high temperature and pressure plasma, generated by the application of high-current, short-lifetime electrical discharge to a polymer capillary, see Figure 1.3.

Interest in plasma ignition of propellants began in the early 1990's and was primarily focused on liquid propellants.[4] Interest in the plasma ignition of solid propellants did not start to develop until several years later, when an enhanced burn rate was thought to have been discovered.[5] Despite the fact that the existence of an enhanced burn rate is still questionable today,[6] it did produce a substantial interest in ETC ignition.
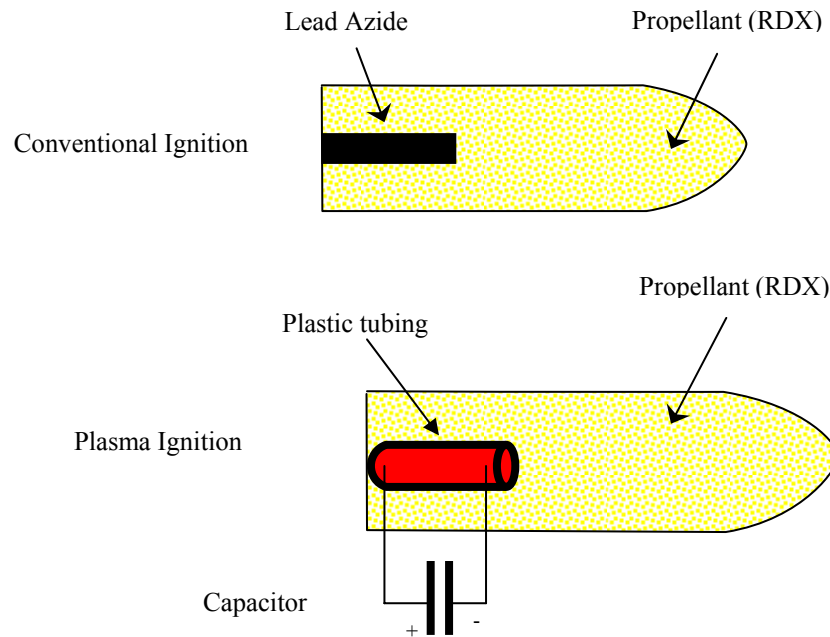
Figure 1.3 – Large bore artillery shell.

Further investigations resulted in the observations of significant advantages of the plasma ignition such as: a short and highly reproducible ignition delay[7] and the possibility of temperature compensation using a trivial adjustment of the electrical energy needed to initiate combustion.[8] Subsequent simulations of the ETC igniter[9] did not explain the benefits, but yielded many insights into the process which was not possible to obtain from the more prevalent studies of pressure transients.

Recent work at the Army Research Laboratory in Aberdeen, MD, has showed numerous observations that may provide significant insight into the process of plasma ignitions. Namely, the studies have showed that the choice of a polymer liner plays an important role in the ignition process. Polyethylene liners, used in the early work, were discovered to leave a residual "soot" on the grains at the time when the detonation was

5

terminated, while plasma ignition achieved with Mylar (polycarbonate) liners left a "clean" surface. Studies of compositional and morphological changes in grains exposed to the ignition source have proved that pits, gouges, blisters and wormholes are formed on the surface of the propellant grains.[10, 11, 12, 13] Moreover, the normal melt layer was found to be either very thin or absent on the plasma-treated grains and the observed denitration was extending 0.5-0.75 mm into the surface depending on the chemical composition of the propellant. All existing experimental data suggest an ablative, rather than a combustive, process occurring during the initial stages of plasma ignition where increased surface area may be an explanation of the increased burn rate.

Attempts to determine the mechanism of plasma ignition include large variety of techniques which test the influence of specific components of the plasma. Some of these studies are as follows: Andreasson and Carlson[14] built a closed vessel cell in which an electrical current is passed through a test charge while ignited and burned. Despite a number of difficulties coming from a poorly reproducible ignition delay, they did demonstrate an existence of a burn rate enhancement with the application of external electrical power. Katulka et al.[15, 16] investigated the power dependence of ignition for a various propellant compositions. They also demonstrated the effects of Mylar and aluminum films on the samples to reduce exposure of the samples to the UV and ion radiation coming from the plasma. The results of these studies are clouded by the reactivity of some of the films, however, some important observations were still made such as the presence of metal clusters from the plasma source on the samples, radiation transmitted through polyethylene films changed the chemical composition of some

6

propellant mixtures, and all the effects depended strictly on the chemical nature of the propellant. Others focused on heat loss,[17] and modeling of the ignition process.[18, 19]

Modeling of a standard plasma ignition system has showed that the flux of species arising from the plasma ignition source is mostly hydrogen and carbon atoms with their ions.[9] Besides the work at Aberdeen, the Army has also supported several groups that are working in collaboration with the ARL group. For example, at Pennsylvania State University a "standard" ETC igniter has designed and constructed. Moreover, their mass spectrometric measurements of the plasma composition as it expands out of the plasma source are providing experimental results which can be compared directly with the modeling.[20] Another group, at North Carolina State University, uses optical probing of the ETC igniter pulse to investigate the shape and temperature profiles of the expanding plasma pulse.[21] Meanwhile, the group at the University of Texas uses optical probing technique to image individual chemical constituents of the pulse.[22]

In order to understand the process of erosion of propellant films in the plasma it is important to understand the physical processes taking place in plasma environment. It is not unreasonable to assume that physical sputtering is responsible for erosion of propellant films in plasma. At the microscopic level physical sputtering can be considered as a result of fast moving ions bombarding a surface which leads to a transfer of entire energy and momentum to the lattice. This process is well known for many types of materials,[23] however propellants are unusual sputter targets. First, they are molecular solids, meaning they are composed of molecular units that are held together by relatively

weak Van de Waals forces as compared to the covalent forces which bind the atoms of the more traditional sputter targets, such as metals and semiconductors. Due to the weaker bonding between the units, molecular solids tend to have higher sputter yields. Second, propellants can spontaneously combust, if sufficient pressure and temperature are achieved. When a propellant surface is impacted by an ion, combustion may become an additional and likely outcome. The mechanism of ion stimulated propellant combustion can be understood through either an atomistic or a continuum model of the interaction. From atomistic point of view, the glancing angle collisions of an ion with a propellant molecule can transfer sufficient amount of energy and momentum to the vibrational and electronic energy manifolds of the propellant molecule to initiate combustion. From a continuum viewpoint, the ion bombardment event may be seen as the source of a short-lived, local pressure and temperature spike as the ion transfers its momentum and energy to the surface. When the spike in pressure and temperature are large enough, local conditions suitable for the spontaneous combustion of propellant molecules can result within a few nanometers of the ion impact point.

Ion energy plays a large role in determining the outcome of the ion bombardment process. The resulting combination of effects as a function of ion energy is the logical consequence of competing factors in the bombardment process: the energy dependent, or more specifically the velocity dependent cross-section for collision and the average energy transferred to target atoms. At very low ion energies (0-50 eV), the ions move relatively slowly and the collision cross-section with surface layer atoms is very large. Hence, all of the ions undergo "hard" collisions with the uppermost surface atomic layer, where they transfer most of their energy to target atoms. However, with little energy in

the ions, the energy transferred to individual target atoms is most likely below the threshold for ejection of target atoms, and only a small fraction of the atoms are ejected. The result is a low sputter yield. As the ion energy is increased within the low energy regime, the velocity of the ions goes up, and thus, the cross-section for collisions with the uppermost layer goes down. In this regime, ions can penetrate as much as a few nanometers into the surface before suffering a hard collision with a target atom. Meanwhile, the average energy transferred to the target atoms also rises and an increasing fraction of the target atoms now have enough energy to be ejected. In the low ion energy ion regime, the sputter yield reaches a maximum. As the ion energy is further increased to the medium and high energy regime, a large fraction of the ions begin to penetrate deep into the surface layer before suffering a hard collision. Despite the fact that the average energy transferred to target atoms is large, they are too deep to be able to escape the solid and the energy is dispersed within the lattice. As a result, the sputter yield decreases. In the medium to high energy regime, implantation of ions takes place over sputtering and other surface effects.

The modeling of the plasma-propellant interactions (PPI) using laser ablation is based on the fact that the laser ablation of plastics, especially the ones used as liner in ETC igniters produces plasma that in many ways resembles the output pulse of the ETC igniters. By laser ablating a polymer film of proper thickness deposited directly on top of a propellant film, a miniature replica of the ETC igniter pulse can be created at the surface of the propellant. As laser ablation process is highly controllable and can be done on a large variety of sizes by focusing and adjusting power of the laser pulse, the

advantage of this approach is obvious since actual ETC igniters cannot easily be miniaturized.[24]

## I.3. LASER ABLATION

### I.3.1 INTRODUCTION

Ablation, in the broadest sense, is removal of material by incident light. In most metals and glasses/crystals the removal is by vaporization of the material due to heat. In polymers the removal can be induced by photochemical changes which include a chemical degradation of the polymer, akin that employed in photolithography. If the removal is by vaporization, special attention must be given to the plume. The plume will be a plasma-like substance consisting of molecular fragments, neutral particles, free electrons and ions, and chemical reaction products. The plume will be responsible for optical absorption and scattering of the incident beam and can condense on the surrounding material and/or the beam delivery optics. Normally, the ablation site is cleared by a pressurized inert gas, such as nitrogen or argon. If the material to be ablated has a poor absorption, such as diamond, a thermally converted form of the material, such as graphite which has relatively good absorptivity, is used to cover the diamond surface with a thin coating. The laser beam will ablate the graphite and in doing so the surface of the underlying diamond will be converted to graphite allowing efficient absorption. Sequentially, graphite is ablated and each newly formed layer of diamond is converted to graphite. The ability of the material to absorb photons limits the depth to which that energy of light can perform useful ablation. Ablation depth is determined by the

absorption depth of the material and the heat of vaporization of the substrate. The depth is also a function of beam energy density, the laser pulse duration, and laser wavelength. Laser energy per unit area of substrate is measured in terms of the energy fluence.[25] The peak intensity and fluence of the laser beam is given by:

Intensity (Watts/cm$^2$) = peak power (W) / focal spot area (cm$^2$)

Fluence (Joules/cm$^2$) = laser pulse energy (J) / focal spot area (cm$^2$)

while the peak power is

Peak power (W) = pulse energy (J) / pulse duration (sec)

There are several key parameters to consider for laser ablation. The first is selection of a wavelength with a minimum absorption depth. This will help ensure a high energy deposition in a small volume for rapid and complete ablation. The second parameter is short pulse duration to maximize peak power and to minimize thermal conduction to the surrounding work material. This is analogous to a vibrating system where the mass is large and the forcing function is of high frequency. This combination will reduce the amplitude of the response. The third parameter is the pulse repetition rate. If the rate is too low, all of the energy which was not used for ablation will leave the ablation zone allowing cooling. If the residual heat can be retained using a high repetition rate, thus limiting the time for conduction, then ablation will be more efficient. More of the incident energy will go toward ablation and less will be lost to the surrounding work material and the environment. The fourth parameter is the beam quality. Beam quality is

11

measured by the brightness (energy), the focusability, and homogeneity. The beam energy is of no use if it can not be properly and efficiently delivered to the ablation region. Further, if the beam is not of a controlled size, the ablation region may be larger than desired with excessive slope in the sidewalls.

Typical laser sources commonly used in surface modifications include Nd:YAG and excimer lasers. Since this work is focused on laser ablation of polymers (polyethylene and polycarbonate) which both absorb light in the UV region, only ultraviolet laser ablation mechanisms are discussed hereafter.

I.3.2 LASER ABLATION MECHANISMS

Laser-induced ablation results from the conversion of an initial electronic or vibrational photoexcitation into kinetic energy of nuclear motion, leading to the ejection of atoms, ions, molecules, and even clusters from a surface. Laser ablation is a sputtering process in which material removal rates typically exceed one-tenth monolayer per pulse; the surface is structurally or compositionally modified at mesoscopic length scales; and particle yields are superlinear functions of the density of excitation. The formation of an ablation plume (a weakly ionized, low-to-moderate density expanding gas cloud) adds to laser ablation the complications of plasma-surface interactions, gas dynamics, and laser-induced photochemistry.

Lasers deposit energy in irradiated surfaces and the near-surface region of the bulk material down to a penetration depth that is characteristic of the laser frequency (or wavelength) and the material. The energy may be deposited either by exciting free

electrons or by exciting electronic or vibrational transitions in atoms, ions, molecules, or optically active defects. The mechanism, density, and lifetime of the induced excitation depend on the electronic structure, composition, surface topography, and defect populations of the irradiated solid as well as on the laser frequency and pulse duration. There are two steps in the mechanism by which UV laser pulses bring the etching of polymer surfaces with a minimum of thermal damage to the substrate.
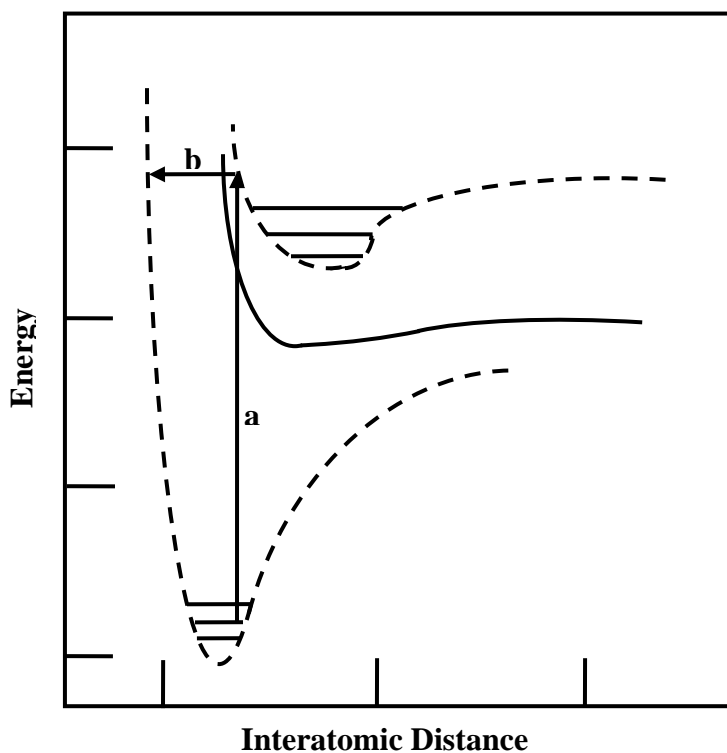


Figure 1.4 - Energy-level diagram for a hypothetical bond A-B. The lower broken line represents the ground electronic state; the upper broken line and the solid line represent excited states.

The principal reaction steps that have been proposed can be understood by referring to an energy diagram, Figure 1.4. It is generally accepted that the absorption of UV photons results in electronic excitation (step a). The excited electronic state can undergo decomposition in that state, which would be a purely photochemical reaction, or, if the

excited molecule undergoes internal conversion (step b) to a vibrationally excited ground state, any subsequent decomposition can be considered to be the equivalent of a thermal process. This is the so-called photothermal mechanism in which the photons merely act as a source of thermal energy.[26]

In Figure 1.5, a schematic diagram of the energy pathways present in ultraviolet processing of polymers is shown. Photochemical and photothermal mechanisms can both lead to decomposition as well as changes in absorption properties. As polymer ablation and modification involves actual chemical transformation of the material, absorption can change with laser processing. Some polymers which are initially only lightly absorbing become absorbing after the first few laser pulses and ablation does not begin until "incubation" is accomplished.[25] The details of surface alteration by laser ablation – such
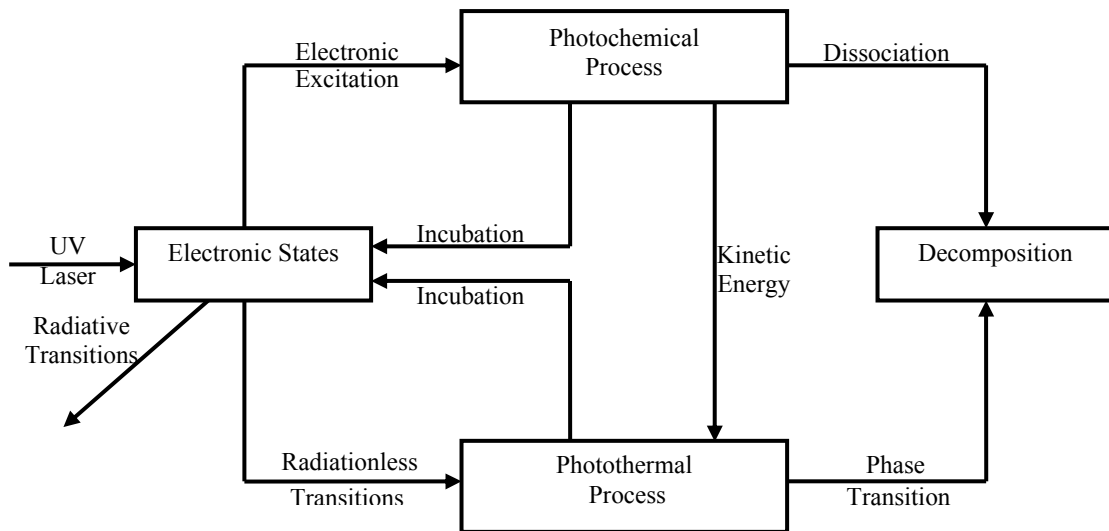


Figure 1.5 – Various energy pathways in UV processing of polymers.[25]

as large-scale material removal – will also be influenced by surface morphology, by surface roughening and instabilities, and by the ambient atmosphere. Finally, the amount

of light absorbed at the surface may be influenced by laser interactions with the ejected material and, in case of thin irradiated samples, by internal reflections and phase changes at internal boundaries.

## I.3.3 LASER ABLATION OF POLYMERS

It is commonly accepted that laser ablation involves photothermal and/or photochemical processes, depending on the nature of the polymers used and the experimental conditions, for example laser fluence, wavelength, and pulse duration. The photothermal process involves the absorption of photons, followed by the release of the photon energy into the polymer matrix via vibrational cooling. This induces a rapid temperature rise in the bulk material leading to the thermal decomposition of the polymer. If the vibrational energy attains a particular fluence threshold, then bonds in the polymer will break, resulting in a phenomeneon known as photofragmentation. These fragments typically occupy a larger volume compared to the surrounding material. The increase in volume, if confined by non-irradiated material below and adjacent to the irradiated material, leads to a sharp increase in pressure and a forward ejection of ablated material. The photochemical process involves the breaking of chemical bonds due to interaction with nanosecond (or shorter), high power, UV pulses yielding gaseous photoproducts. During this process, thermal and mechanical damage to the surrounding polymer is minimal and more precise control over the ablated region is realized.

The ablation of the surface of a polymer by a UV laser pulse is a function of the energy deposited in the solid in unit time. If a typical UV pulse has a full width at half-maximum (FWHM) of 20 ns and an energy of 450 mJ and the size of the beam at the polymer surface is 1.5 cm$^2$, the fluence at the surface will be 300 mJ/cm$^2$ and the power density will be 15 MW/cm$^2$. When this pulse strikes the surface a loud audible sound will be heard and depending upon the wavelength, 0.01-0.1 micron of the material can be removed with a geometry that is defined by the light beam. If this experiment is performed in air, a bright plume will be ejected from the surface and will extend to a few millimeters. Figure 1.6 shows images of laser ablation plumes from polycarbonate films using different laser focusing conditions. In Figure 1.6 (a), the ablation plume can be readily seen. The mushroom cloud like appearance of the plume is the result of emission from the ablated species and the fireball that results when the plume materials combust in



a                                        b
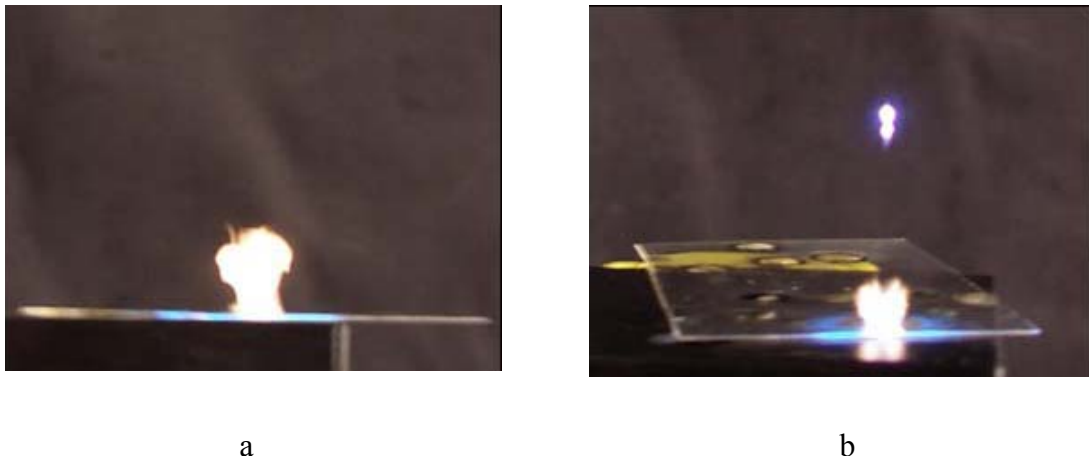
Figure 1.6 – Laser Ablation Plume.

the air. In Figure 1.6 (b), the bright spot in the air is light from the ionization of air at the focal point of the laser.

Typically, UV laser ablation is carried out with a succession of pulses. R. Srinivasan and Bodil Braren[27] have shown that the depth etched is a linear function of the number of pulses and that there is a very long extrapolation between the origin (zero pulses) and the first data point.
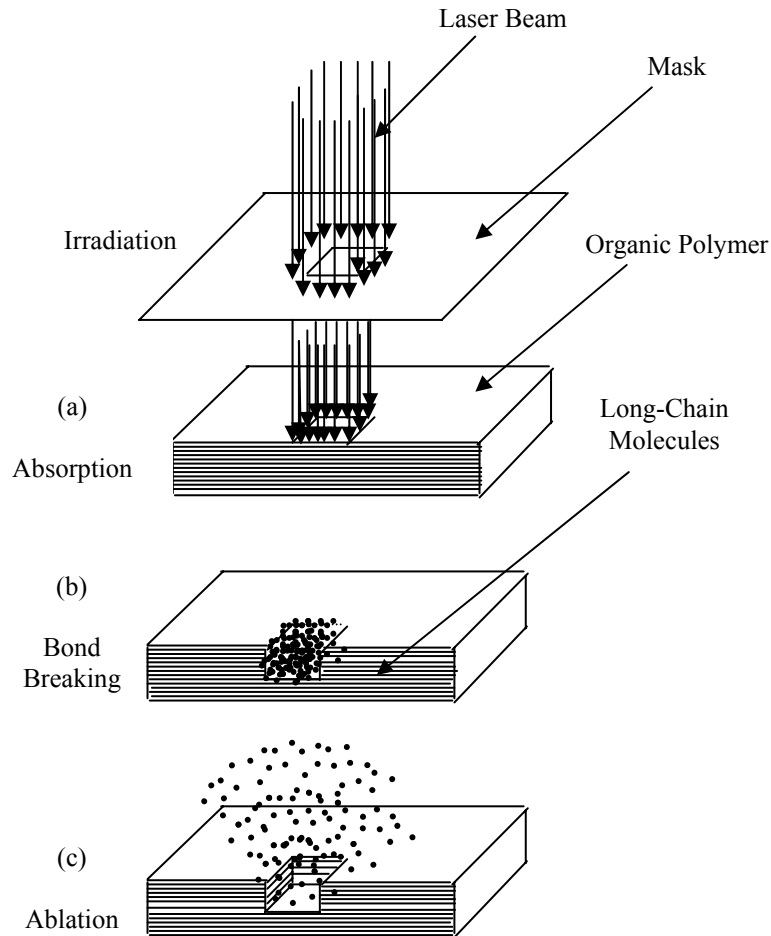


Figure 1.7 – Schematic impact of laser pulse on polymer surface.

A pictorial representation of the interaction of a laser pulse with a polymer surface is shown in Figure 1.7. As shown in Figure 1.7 (a), the stream of photons from a single laser pulse falls on the polymer and is absorbed in a depth that can he as little as a

fraction of a micron for intense absorbers, to many tens of microns for weakly absorbing polymers. Obviously, weak absorption and strong absorption refer to specific wavelengths so that the same polymer can absorb weakly at one laser wavelength and strongly at another. Figure 1.7 (b) shows that within the absorption depth, there are numerous bond breaks. In Figure 1.7 (c), the fragments are shown to be ejected from the surface, leaving an etched pit behind.

The general features of UV laser ablation of polymers are summarized as follows:

- Polymer ablation takes place within 10 to 100 nanoseconds.

- The threshold energy fluence, defined as the fluence at which the etch depth is 0.05 μm per pulse, is low for polymers (typically in the range 10 to 100 MJ/cm$^2$).

- For fluences near or below the threshold, the etch depth follows Beer-Lambert's law (photo-chemical, linear absorption). For fluences above the threshold, thermal effects contribute to the etch depth. In addition, the longer the wavelength, the stronger are the thermal effects.

- Wavelength affects absorption and threshold fluence. The etch depth per pulse (lower absorption coefficient) is larger for a weaker absorber than for a stronger absorber.

- The formation and expansion of the plasma plume during the laser pulse characterize the rapid etching process. The etch depth per pulse increases with

energy fluence until the phenomenon of saturation is reached. "Saturation" is a mechanism involving the blocking of the trailing part of the laser pulse by both the plume and the excited polymer species generated by the leading part of the pulse. This occurs only at high energy densities and prevents additional material removal.

- Ablation is accompanied by an acoustic signal that decreases with increasing laser wavelength.

- Ablation creates numerous products, which may include atoms, monomers and fragments normal to the surface. The velocities of ablation products are high, up to 101 m/s. The velocity distribution of ejected material is not dependent on the energy fluence.

- Ablation takes place in the temperature range 400 to 800 $^0$C.

- The small absorption depth coupled with short laser pulses and low thermal conductivity of polymers restricts the extent of heat transfer, leading to precise material removal and a small heat-affected zone.

I.3.4 LASER ABLATION OF RDX FILMS

When a sample is illuminated with a short pulse of intense laser radiation, a few monolayers of material may be "cleanly" removed from the surface, see Figure 1.8.



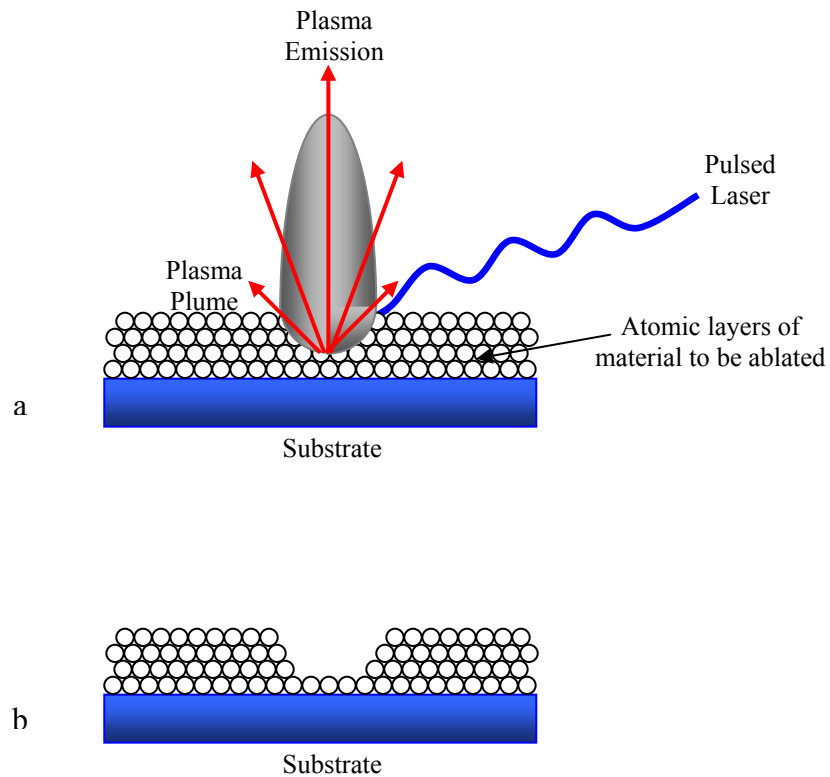Figure 1.8 – a) Ablation of material; b) Sample after ablation.

In laser ablation, the rapid adsorption of laser energy generates a high-pressure, high-temperature plasma that then extinguishes rapidly as it expands into the ambient environment, see Figure 1.8 (a). Experimental measurements and theoretical studies of laser ablation both indicate that pressures of several MPa and temperatures of several

thousand degrees are typically realized in the ablation process.[28,29] Hence, it is no coincidence that images of laser ablation plumes closely resemble the plumes recently observed by Varghese[30] observed to emerge from an ETC ignition source.

In this work, the laser ablation of thin films of ETC liner material deposited directly onto propellant samples is studied. Polyethylene and polycarbonate films are typically used by the Army as ETC liners and have been shown to be effective igniters when ablated, consequently they have been chosen for study herein. Ablation of both of these polymers can be achieved with UV irradiation with the fourth harmonic of an Nd-YAG laser. Ablation of deposited layers of these polymers will produce short-lived plasma very similar to those found at the exit ETC igniter.

Finally, it should be noted that the ablation process removes only a few monolayers (see Figure 1.8) of material at a time and that the deposition of the films will most likely result in thickness on the order of microns. Therefore, a single pulse ablation experiment will simply measure the ablation products of the bulk films. However, repeated ablation of the same region, using a laser spot size of ~ 1mm as compared to the micron thickness, will successively thin the film until pure propellant is revealed. When the polymer film thickness exactly matches the ablation depth, the surface of the propellant will be presented with plasma comparable in composition and pressure to the output of an ETC igniter. Under these conditions, the propellant is expected to burn at least until the pressure of the ablation pulse dissipates. For identically ablated structures where the polymer film is 10-20% thicker, the ablation will not reach the surface of the propellant and only the pressure of the pulse, but not the chemical species of the plasma,

will reach the surface of the propellant. In this case, the propellant film is expected to remain mostly intact after the laser pulse. For structures that have polymer films 10-20 % thinner than the ablation depth, some of the propellant will be expected to ablate directly, a process that has been shown not to be capable of igniting the propellant.[16]

## I.4 THIN PLASTIC FILMS

## I.4.1 DEPOSITION METHODS

Spin-coating has been extensively exploited by the microelectronics industry for depositing layers of photoresist films on to silicon wafers. [31] The various steps involved in the process are illustrated in Figure 1.9. A quantity of a polymer solution is first placed
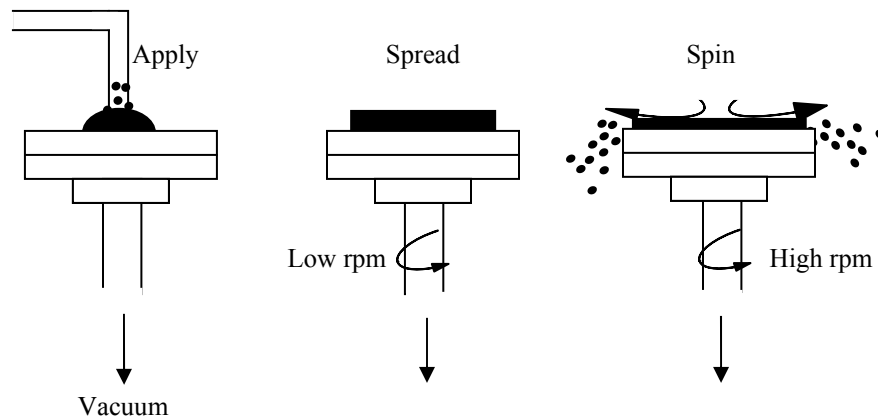


Figure 1.9 – Spin-coating technique.

on the substrate (typically semiconductor wafer), which is then rotated at a fixed speed of several thousand rpm (or the solution can be applied while the wafer is slowly rotating).

The resist solution flows radially outwards, thus reducing the fluid layer thickness. Evaporation of the solvent results in a film of uniform thickness. The initial stage involves delivering a quantity of solution to the surface of the substrate. The polymer viscosity (dependent on the concentration of the starting solution) and final film speed are both important process parameters. An increase in angular velocity decreases the film thickness; an inverse power-law relationship usually holds for the thickness dependence on the final spin speed. For a given speed, the film thickness decreases rapidly at first, but then slows considerably at longer times. A simple theory[32] predicts the following relationship between the thickness of the spun film, d, the viscosity coefficient of the solution, $\eta$, its density, $\rho$, the angular velocity of the spinning, $\omega$, and the spinning time, t:

$$d = (\eta/(4\pi \rho \omega^2)^{1/2}t^{-1/2} \qquad (3)$$

Organic compounds that have been successfully deposited by spin-coating include electrically insulating polymers such as poly (vinylidene fluoride), conductive polymers and dyes developed for electroluminescent displays, and certain phtalocyanine materials.[33, 34, 35, 36, 37] Although spin-coating is expected to produce films in which individual molecules are relatively disordered, this is not always the case. For example, organized phtalocyanine layers have been deposited.[35] The way in which the order is achieved is not fully understood but may result from the centrifugal forces acting upon the individual molecules during spinning. Spin-coating is the preferred method for application of thin, uniform films to flat substrates.

Other methods of thin film formation include dip-coating, spraying, painting, and screen printing. Most of these techniques are relatively easy to carry out and require a minimum of equipment. Polymer films of materials such as polypropylene, polystyrene

and poly(vinyl chloride) (PVC) can be obtained by the technique of direct isothermal immersion of a substrate into a suitable solution of the polymer (e.g. PVC in cyclohexanone). Material will be deposited on the immersed substrate until equilibrium is reached between the deposition rate and the re-solution rate. Satisfactory films can also be obtained by solution casting – allowing the evaporation of a polymer-containing solution placed on a substrate (e.g. polystyrene in chloroform).

The technology of screen printing offers a further inexpensive method for the preparation of films. The process consists of dispensing a paste (the ink) of the material to be deposited on a mesh-type screen on which a desired pattern may be defined photolithographically. The substrate is placed at a short distance beneath the screen. A flexible wiper then moves across the screen surface, deflecting it vertically and bringing it into contact with the substrate. This forces the paste through the open mesh areas. The substrate is allowed to stand at ambient temperature for some time in order to enable the paste to coalesce to form a coherent film.[32]

In the spraying method, a polymer solution is typically sprayed onto a pre-heated substrate. The thickness of the coating is governed by the total exposure time and the concentration of the spraying solution. In our case, the film thickness is controlled by the number of repeated passes of the spray across the substrate. A large particle size originating from insufficiently soluble polymers or a wide molecular weight distribution may facilitate the formation of numerous heterogeneities within the microstructure of the coating. In this work, polyethylene powder is only partially dissolved in a solvent (toluene) to form a saturated solution which is then used to spray on to a pre-heated

substrate. The resulting thin films often have a rough surface with inconsistent thickness measured in different spots. In fact, the thickness can vary over the surface the film by as much as 50 %.

## I.4.2 THIN FILM CHARACTERIZATION

Two main characteristics of polymer thin film quality are film hydrophobicity and uniformity. The first parameter can be estimated by measuring a contact angle (the angle at which liquid/vapor meets the solid surface), see Figure 1.10.
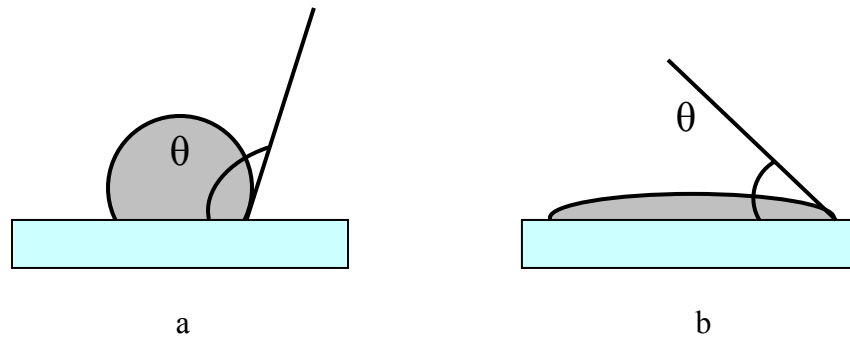


Figure 1.10 - Contact angle.

Figures 1.10 (a) and 1.10 (b) demonstrate a difference in wettability. Figure 1.10 (a) shows how a water droplet might appear on a hydrophobic surface such as wax. Figure 1.10 (b) shows how a water droplet might appear on a hydrophilic surface.

To evaluate the thin film uniformity, various techniques such as optical microscopy, scanning electron microscopy (SEM), transmission electron microscopy (TEM) as well as scanning probe microscopes – AFM, STM, etc. can be employed. In

this work, to evaluate the surface uniformity, a water droplet is placed on a surface of polymer coated glass slide: if the surface is uniform, the droplet is observed to roll freely over the entire surface of the film as the slide is tipped. To confirm the reliability of the technique, SEM images were also obtained.

# II. EXPERIMENTAL

## II.1 THIN PLASTIC FILMS

### II.1.1 INTRODUCTION

Electrothermal Chemical (ETC) ignition is a new technology based on the generation of a high temperature and pressure plasma by the capacitive ablation of a polymer liner. Polyethylene and polycarbonate are two of the more common polymers used in ETC research. Efforts to develop spray-on technologies of polymer films have been focused on the preparation of polyethylene and polycarbonate films, to correlate with the ETC igniters used by the ARL (Army Research Lab) group and Varghese,[30] respectively. In the spraying method, a polymer solution is sprayed on to a pre-heated substrate and the thickness of the coating is governed by the number of repeated passes of the spray across the substrate. Another common technique of forming thin polymer films is spin coating. In the spin coating method, a quantity of polymer solution is placed on the substrate which is then rotated at a fixed speed. To prepare smoother, more uniform polymer thin films, it would be preferable to develop spin-coat technologies for both polyethylene and polycarbonate.

Film quality was judged by several standards. The first standard was the

hydrophobicity determined by the contact angle of 10 µL water droplets placed on the films. Figure 2.1 shows 10 µL water droplets placed on a microscope slide covered with polycarbonate film (right) and on a droplet placed on a microscope glass slide without film (left).



Figure 2.1 – Water droplets placed on a microscope slide covered with polycarbonate film (right) and on a droplet placed on a microscope glass slide without film (left).

In this work, the contact angle is defined as the angle between the surface and the rising edge of the droplet. A film judged as good is less than 90 degrees, while, in poor quality films, the angle may be as large as 140 degrees, see Figure 2.1. The second standard was the presence of pinholes. This was determined in one of two ways. If pinholes exist, the droplet is observed to adhere to an individual point on the surface as the sample is tipped. If pinholes are not present the droplet freely rolls across the surface as the slide is tipped. Another test for pinholes is the stability of the surface to the presence of water drops. If pinholes exist, water seeps through them and below the film to wet the hydrophilic glass surface. This undermines the film and in a matter of minutes the film tears and the droplet



Figure 2.2 – Polycarbonate film with pinholes

28

appears to be below the fragments of the film, see Figure 2.2. To confirm the reliability of these tests, SEM images were also taken, see Figure 2.3.



a                                                                                    b
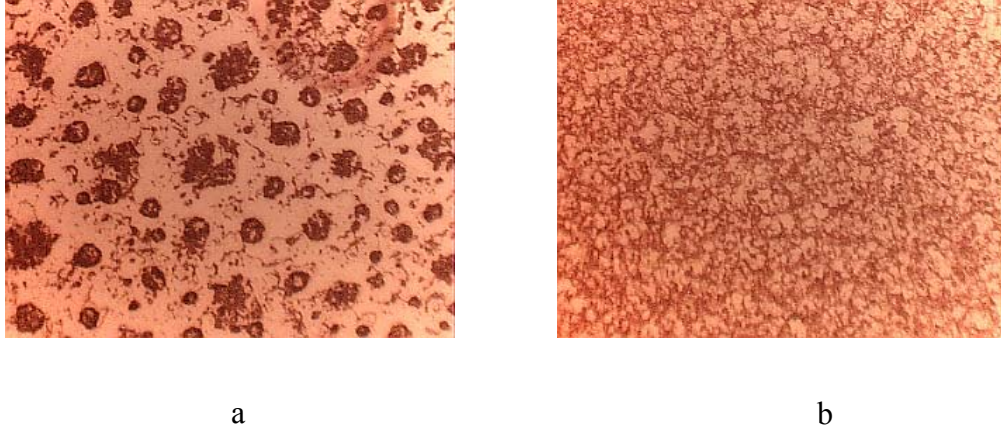
Figure 2.3 – SEM images of polyethylene films: a) film with pinholes; b) film without pinholes

The thickness of the films has been measured by using a Tencor Alpha-Step 200 surface profiler. The device measures surface profiles by means of scanning a mechanical stylus across the sample. The small motions of the stylus are amplified and displayed as a chart on the computer. The thickness of the film is then determined as a difference between two points: the surface height of the glass slide covered with polymer and the surface height of the glass slide alone.

## II.1.2 EXPERIMENTAL SETUP

SPRAYING TECHNIQUE

A 50 ml round bottom flask is attached to the sprayer unit using a standard 14/20 ground glass joint and is secured by rubber bands see Figure 2.4. The sprayer has a thick wall 1.5 mm I.D. feed tube that extends ~ 40 mm from ground glass, is bent 90 degrees and terminates in a 0.5 mm capillary. The capillary feeds through the wall of a 15 mm I.D. closed-end tube that extends ~ 60 mm above the joint. The outer closed-end tube has both a feed port for $N_2$ pressurization and an opening in the side for pressure relief. No sheath gas is designed into the sprayer as the polymer solutions are at, or near, saturation and any significant loss of solvent would inhibit flow of the droplets once on the substrate surface, resulting in rougher films.
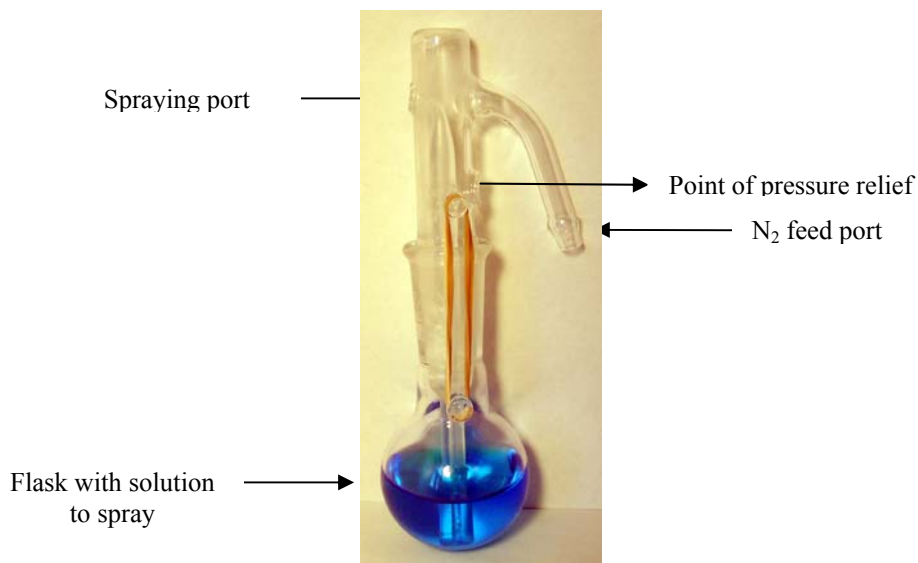


Figure 2.4 – Sprayer. (Note that the food dye was added to allow the reader to see the normally colorless solution)

To spray a film, the round bottom flask is filled with polymer solution, the sprayer is attached, a $N_2$ flow is applied, and the pressure relief opening is covered with a finger, see Figure 2.5. The glass substrate is heated to ~ 100 °C.



Figure 2.5 – Spraying technique.

SPIN-COATING TECHNIQUE

To prepare thin films by spin coating, a Laurell WS-400 B spin-coater device was used. After a substrate is loaded on to the chuck, vacuum hold-down is engaged from the side mounted control panel and the lid is closed, a pre-programmed process is selected and then initiated. A 1 ml of polymer solution is placed on the substrate. The spin-coater was programmed to operate in 2 stages. Stage one is a spin coating with a revolution rate of 500 rpm for 5 seconds. Stage two was programmed to spin coat for 45 seconds with a

revolution rate of 1500 rpm. The first stage was necessary to insure that the polymer



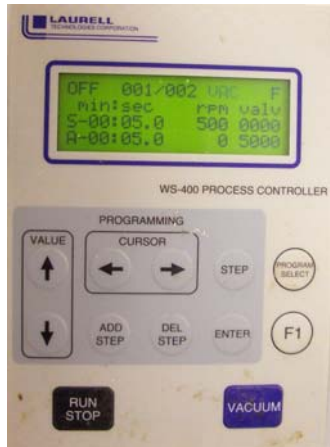solution coats uniformly and is not lost to walls of the device. The program panel is shown on Figure 2.5.

Figure 2.6 – Spin-coater WS-400 Process Controller.

## II.1.3 SPRAYED-ON FILMS

Polyethylene films were sprayed from a nearly saturated solution, typically 0.01364 g/ml, in toluene. The solutions were prepared by adding a pre-weighed quantity of polyethylene powder (Alfa Aesar A10239 and Acros 178505000) to 30 ml of toluene, and refluxed for several hours or overnight to insure dissolution of the solid. Polyethylene solutions with concentrations significantly higher than 0.014 g/ml were too viscous to spray and therefore were not used. Solutions with concentration significantly lower than 0.0135 g/ml formed discontinuous films that had numerous pinholes. Images of 8.2 μm thick polyethylene films sprayed-on at room temperature and at ~100 °C are shown in Figure 2.6. Polyethylene films sprayed onto room temperature glass slides did not pass any of the tests for a high quality film. These films appeared an almost opaque

white. They were insufficiently hydrophobic and riddled with pinholes.



Figure 2.7 - Polyethylene films sprayed at room temperature (left) and at ~100 °C (right).

Films sprayed onto glass slides heated to ~ 100 °C, as measured with an optical pyrometer, appeared more transparent and proved to be very hydrophobic, and displayed no evidence of pinholes. Spraying at temperatures significantly above 100 °C resulted in
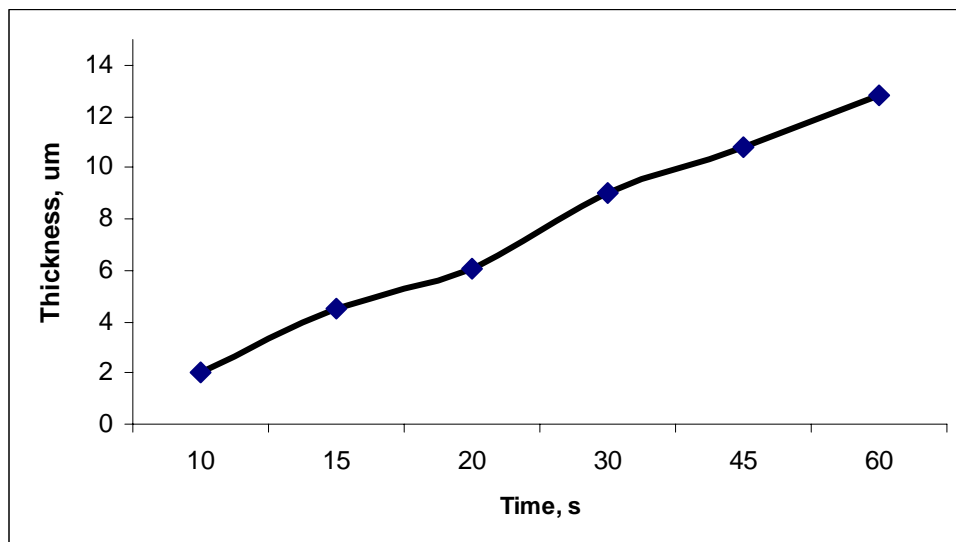


Figure 2.8 - Thickness of sprayed-on polyethylene films as a function of spraying time.

instant melting of the polymer film. Figure 2.8 is a plot of the thickness of the resulting films as a function of spraying time.



Figure 2.9 – Polyethylene film alone (top) and polyethylene film with underlying RDX film (bottom) placed on a glass slide.

Polyethylene films have also been sprayed onto glass slides where RDX films had previously been prepared. The spraying of the polyethylene films had no visually detectable effect on the morphology of the underlying RDX film, see Figure 2.9.
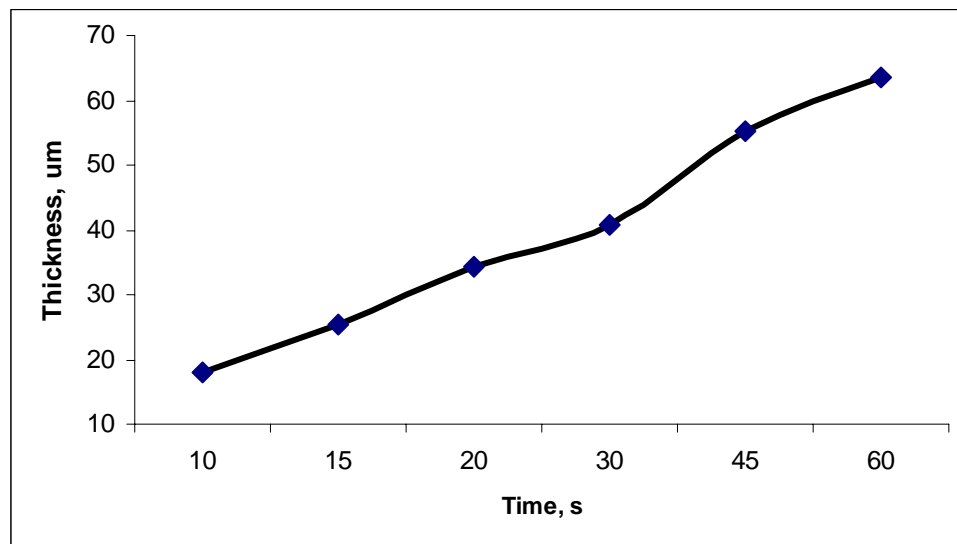


Figure 2.10 - Thickness of sprayed-on polyethylene films as a function of spraying time

Polycarbonate films were prepared from a pre-weighed amount of cut

polycarbonate sheet (McMaster Carr 10mil, 85585K13) that was dissolved in 99.5% methylene chloride (UN 1593 Acros) to yield a solution of 0.023 g/ml. Solutions with concentrations significantly smaller than 0.023 g/ml failed to form a good quality film, while solutions with concentrations significantly higher than 0.023 g/ml were too viscous to spray. Pinhole free, hydrophobic films of polycarbonate can be prepared by spraying onto a glass slide heated to ~ 100 °C. Room temperature polycarbonate films were significantly less hydrophobic and had a large number of pinholes. Figure 2.10 is a plot of the thickness of the resulting films as a function of spraying time. The morphology of a sprayed-on polycarbonate film closely resembled the morphology of the polyethylene films sprayed onto a ~ 100 °C substrate, see Figure 2.11. Polycarbonate films have also been sprayed onto glass slides where RDX films had previously been deposited. The spraying of the polycarbonate films had no visually detectable effect on the morphology of the underlying RDX film, see Figure 2.11.



Figure 2.11 - Polycarbonate film alone (top) and polycarbonate film with underlying RDX film (bottom) placed on a glass slide.

## II.1.4 SPIN-COATED FILMS

None of the efforts to spin-coat polyethylene films have been successful. Spin coating from solution resulted in highly discontinuous films that appeared to have crystallized at the surface of evaporating solvent droplets. This is primarily due to the low solubility of polyethylene in all solvents investigated. In an attempt to spin-coat molten polyethylene, a custom top cover for a spin coating device was made, see Figure 2.12. Heater wire was connected to form spirals around the glass tube to ensure melting of the polyethylene. Once the melting point is reached the polyethylene granules, which
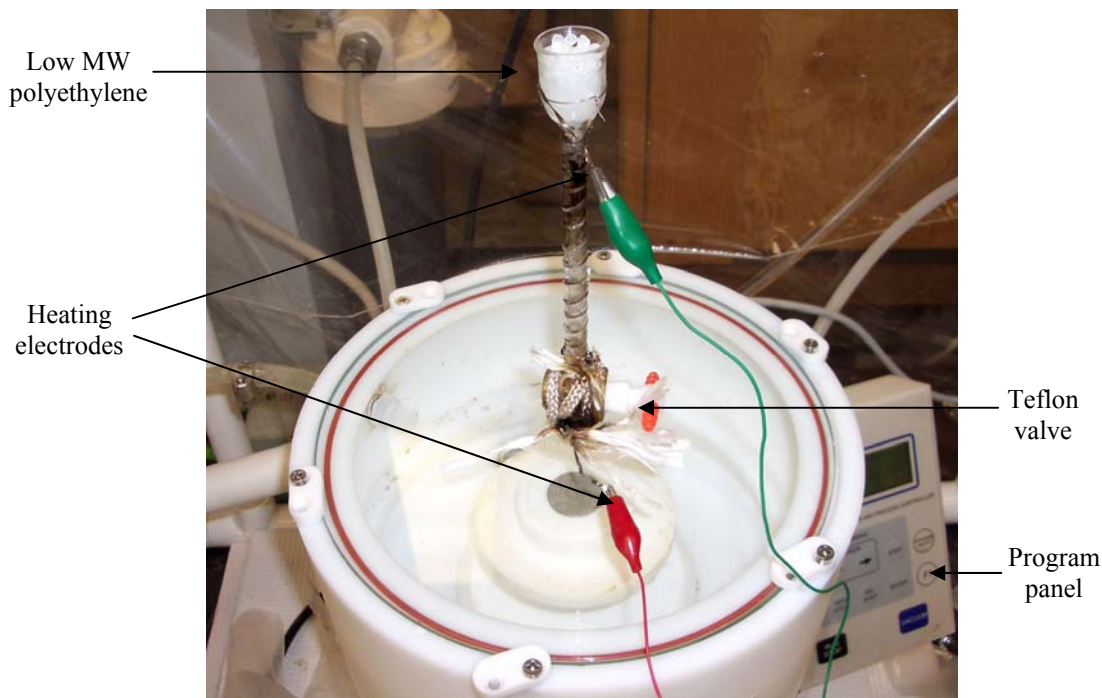


Figure 2.12 – Spin coating from a molten polyethylene.

are supplied from the top opening, start to melt down the tube and the Teflon valve is opened allowing molten polymer to spin coat the glass slide.

All attempts to spin-coat from molten polyethylene produced only thick string-like deposits (see Figure 2.13), presumably due to the high viscosity of the polymer, even using the low molecular weight (M.W. 50,000 Acros) material.
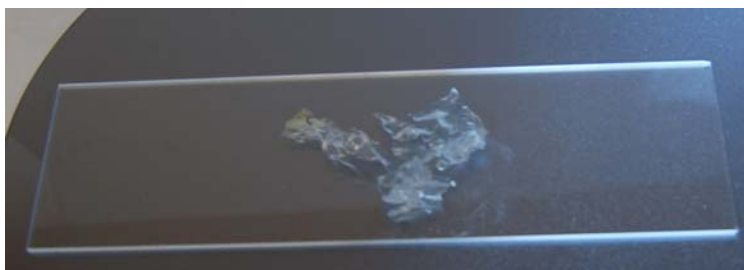


Figure 2.13 - Molten polyethylene spin coated on a glass slide.

Polycarbonate films were readily prepared by spin-coating from methylene chloride solutions of various concentrations. The resulting films were smooth, continuous, hydrophobic and pinhole free, see Figure 2.14.
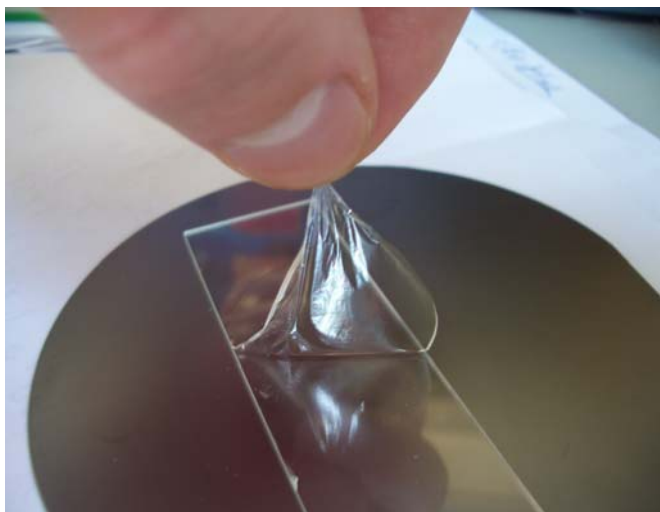


Figure 2.14 – Spin-coated polycarbonate partially removed from the glass slide.

The film thickness can be varied by controlling the rate of revolution, see Figure 2.15.
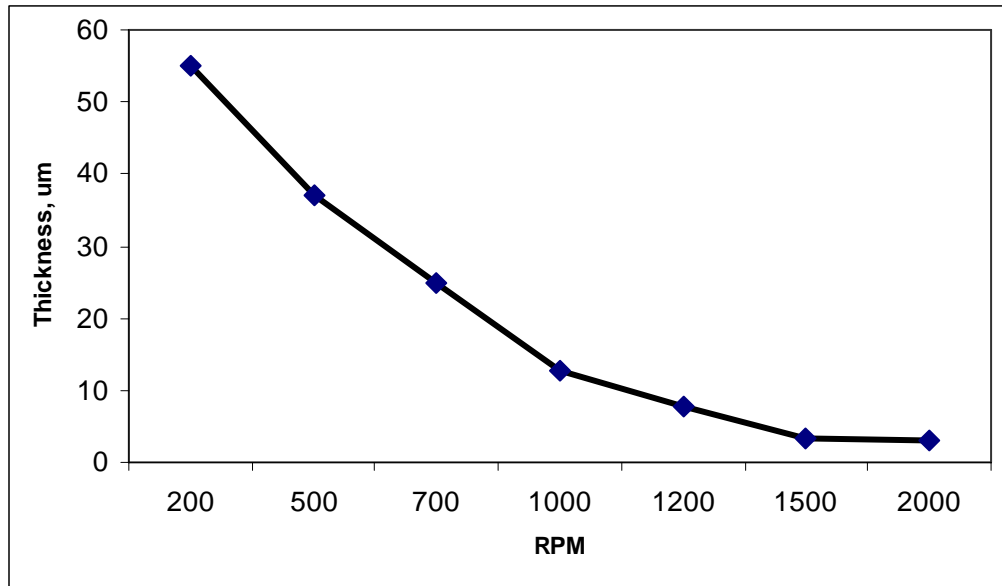


Figure 2.15 – Thickness of polycarbonate films as a function of revolution rate.

In order to choose the optimum revolution rate, a polycarbonate solution with a concentration 0.005 g/ml was chosen to spin-coat at various rpm settings, see Figure 2.15. Solutions with concentrations significantly smaller than 0.005 g/ml failed to form a thin film, and the solution simply was wasted on the walls of the device. The thinnest polycarbonate film yielding a thickness of 3 μm was obtained at 1500 rpm, see Figure 2.16. Once the optimum rate of revolution of 1500 rpm was determined, the effect of concentration was investigated, see Figure 2.16. The spin coater was programmed to perform an operation in two steps. First step is to spin coat for 5 seconds at a rate of 800 rpm, and then to spin coat for 45 seconds at a constant rate of 1500 rpm. The first, reduced-rate step is necessary to avoid wasting of the solution on the walls of the device. So the revolution rate of ~ half of the constant rate was chosen for the first step.
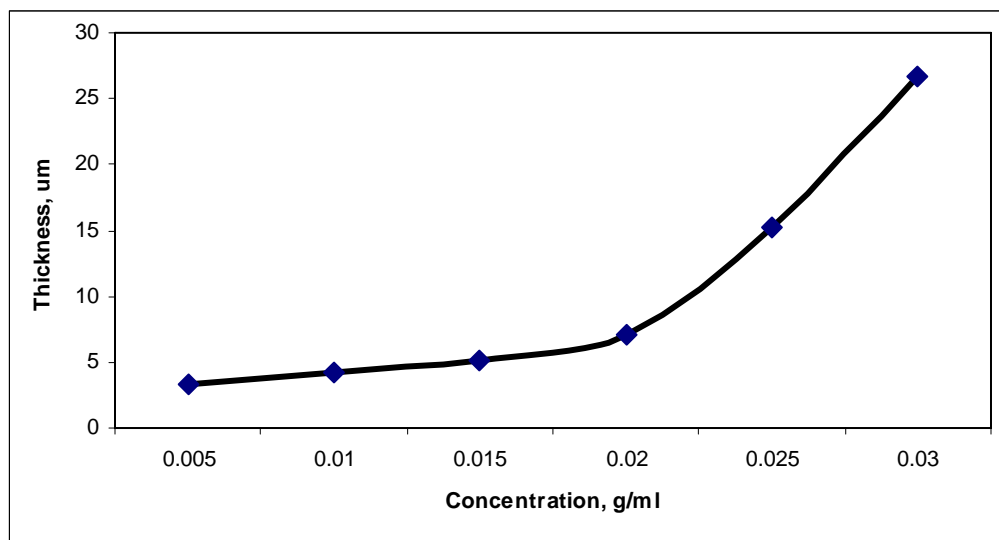
Figure 2.16 – Thickness of spin-coated polycarbonate films as a function of concentration.

Polycarbonate films have also been spin-coated onto glass samples where RDX films had previously been prepared. The spin-coating of the polycarbonate films had no visually detectable effect on the morphology of underlying RDX films, see Figure 2.17.



Fig. 2.17 - Polycarbonate film alone (top) and polycarbonate film with underlying RDX film (bottom) placed on a glass slide.

39

CONCLUSION

Overall, the spin coating method resulted in higher quality polycarbonate films in terms of uniformity and hydrophobicity 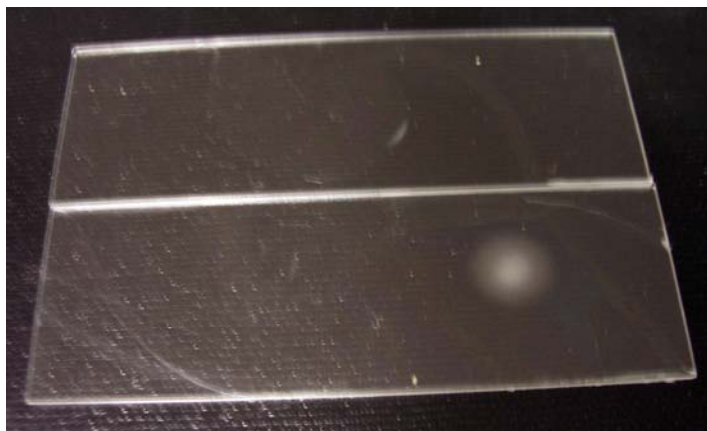as opposed to the spraying technique. The films were significantly thinner (~ 10 fold) with virtually constant thickness over the surface of the film and pinholes free. The thickness of polyethylene sprayed-on films was comparable to the one of spin-coated polycarbonate films. However, due to inaccuracy of manual spraying, uniformity of the sprayed-on films remains an issue. The thickness of the sprayed-on films measured by profilometer varies over the surface of the film by ~ 50%.

The possibility of enhancing the film properties by adding commonly used plasticizers such as phthalate esters to the polycarbonate solutions was also investigated. No difference in film quality or thickness was observed after adding a plasticizer. Since spin-coated films proved to be of a higher quality than sprayed on films, only spin-coated polycarbonate thin films are used in this work in laser ablation experiments.

II.2 LASER ABLATION OF RDX FILMS

II.2.1 DEPOSITION OF RDX FILMS

Initial attempts at preparing thin film samples by filling a reservoir with an analytical solution of RDX and evaporating the solvent resulted in very uneven films that tended to be very thick at the edges of where the final drops of liquid solution existed,

and nonexistent on other parts of the sample holder. It was decided that a spray deposition system would be superior in both film uniformity and quantification of the amount of film deposited. The nebulizing spray system[38] designed was based on the design of a typical nebulizer found in an electrospray mass spectrometer. In this design, a solution is slowly driven through a thin tube that is run down the center of a larger diameter tube that carries a much faster moving sheath gas. As the solution emerges from the small tube, the much faster moving sheath gas breaks it down into small droplets. As the droplets are carried to the sample in the sheath gas, a significant fraction of the solvent evaporates into the "dry" sheath gas. Under the deposition conditions described below, the RDX appears to be deposited almost completely dry. This is interpreted to mean that, as the solvent is removed in the sheath, the solution concentration increases to the solubility limit and crystallization may begin within the sheath as the droplet is carried to the sample.

EXPERIMENTAL

A nebulizing sprayer was constructed from a standard 1/8" swagelock Male Run Tee NPT adapting tee, see Figure 2.18. The noncollinear swagelock connection is attached to source of nitrogen and is used to provide the gas sheath. A rubber septum is attached to the 1/8" NPT connector and is secured with a twisted piece of wire. A 1.5" piece of 1/16" tubing is epoxied into one end of a 1.5" length of 1/8" steel tubing such that ~1/8" sticks out, and the other end is attached to the collinear swagelock connector. One end of a one foot length of 32 gauge (0.009" O.D., 0.004" I.D.) tubing is inserted
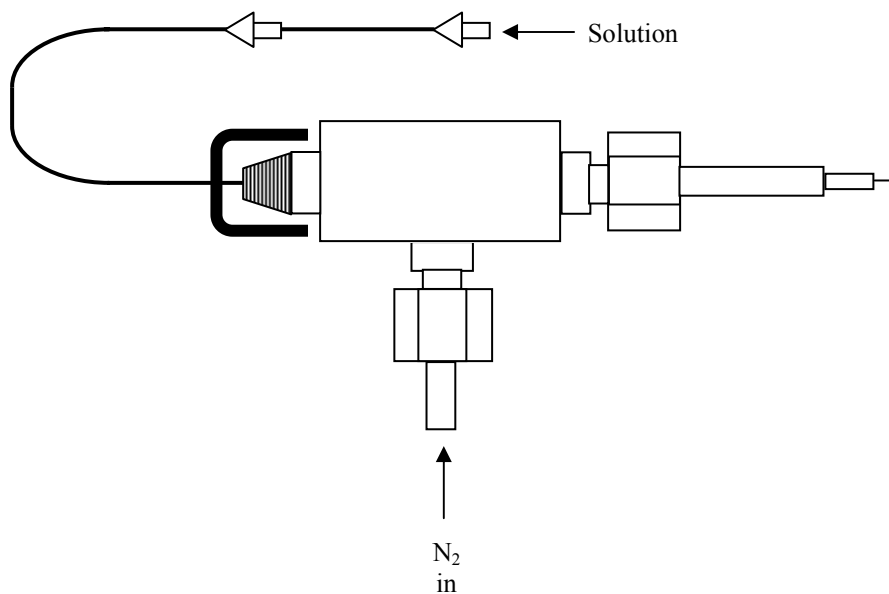
41

Figure 2.18 – Nebulizing Sprayer.

into a 26 gauge syringe needle with epoxy and the other end is inserted through the
septum using a second syringe needle which is withdrawn back onto the tubing after the
tubing has been fed ~ 1/8" out of the end of the 1/8"-1/16" tube on the other end of the
adapter. A 1 ml syringe is then filled with 1000 µg/ml RDX in acetonitrile solution. The
solution is then driven through the 32 gauge tubing at a rate of 1.5 ml/hour as the $N_2$
sheath gas is flowed from a pressure of 40 psi.

II.2.2 CALIBRATION

A Continuum Inlite Laser Nd-YAG, 4 ns pulse, 50 mJ/pulse @ 266 nm is used in
ablation experiments, 10 mil (0.254 mm) thick films of polycarbonate were obtained
from McMaster Carr (85585K13), and 1000 µg/ml analytical samples of RDX in

acetonitrile obtained from Cerilliant.   In terms of ablation of polycarbonate, the laser was more than adequate. Laser fluence at the surface of the film, the critical parameter for ablation, was adjusted at full laser power (a Q-switch delay of 190 μs and 1300V on the flashlamps) by simply focusing the beam by adjusting the distance between the sample and a 110 mm focal length lens.  Polycarbonate films could be ablated from full focus, 110 mm separation, up to a spot size of ~1 mm, which was ~1/2 the beam size at unfocused separation.  The unfocussed laser beam, or laser focused to a spot size of >1 mm resulted in no ablation or other effect on the film. The size of the ablation pits and the number of pulses necessary to break through the polycarbonate film were determined as a function of separation between the sample and the lens, see Figures 2.19 and 2.20. The data were taken using a 190 Q-switch microsecond delay.
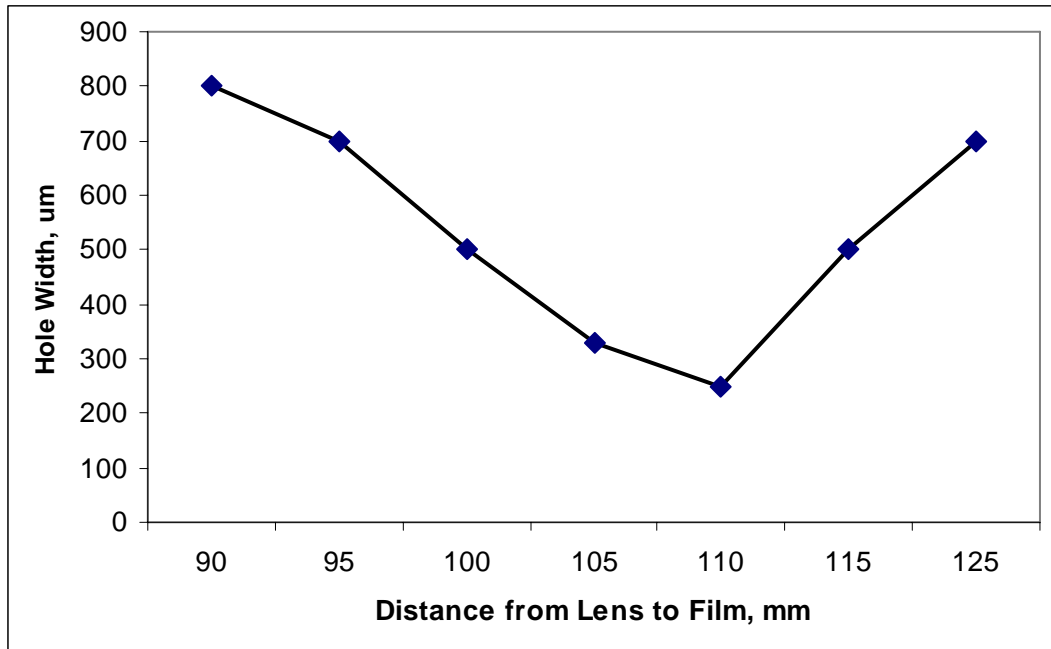


Figure 2.19 – Polycarbonate film hole width as a function of lens to film distance.

The optimal focus conditions were found at a lens to sample distance of 110 mm. At this
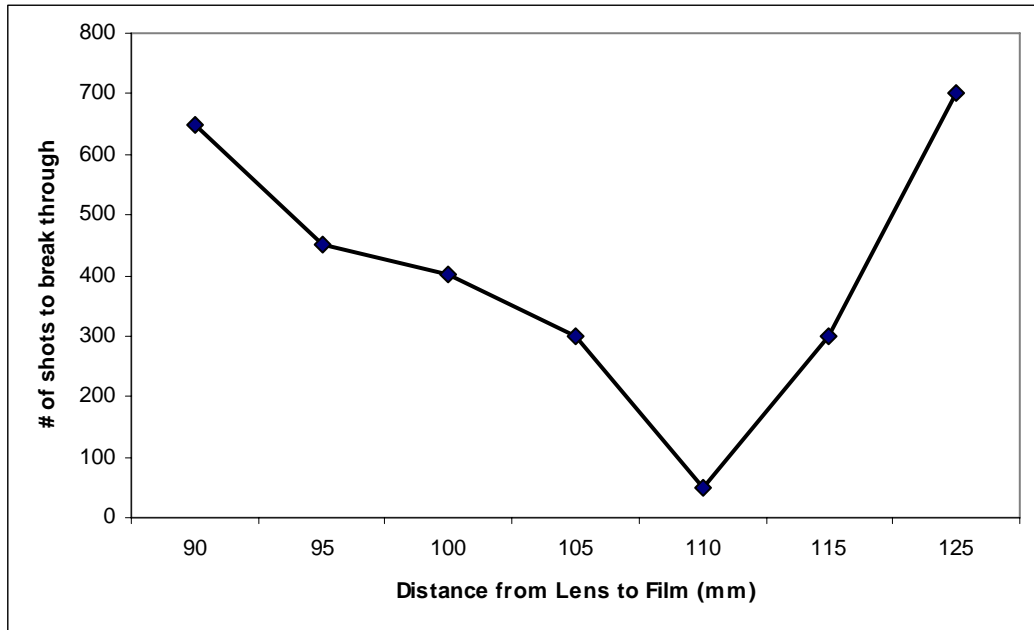


Figure 2.20 – Number of shots necessary to break though a 0.254 mm thick polycarbonate film as a function of lens to film distance.

distance the smallest number of shots (20) is necessary to breakthrough the film, which also produced the smallest hole of 0.25 mm.

Figure 2.21 is a photograph of ablated polycarbonate films. The discoloration observed on the film around the ablation pits is soot from the fireball created by the ablation event that can be wiped from the surface with methanol. For the purposes of this picture the soot has been left on the film to help provide image contrast.

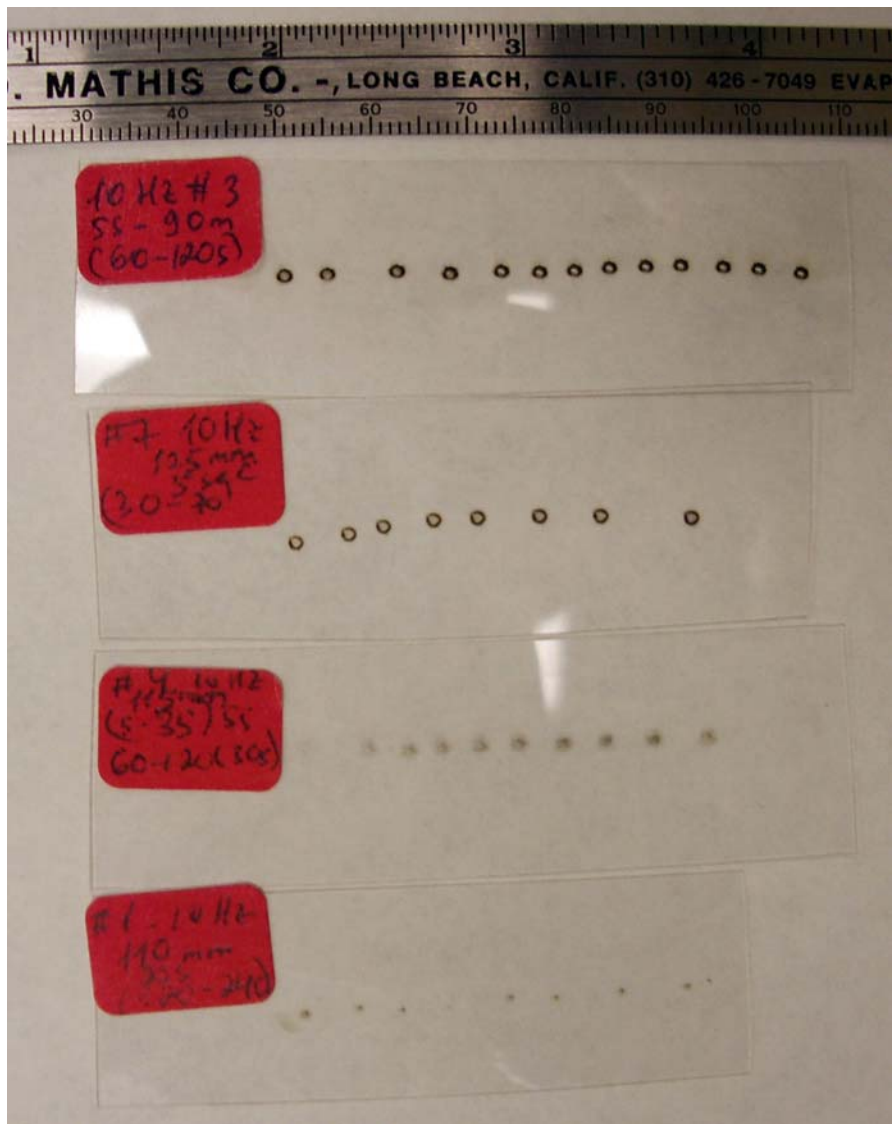Figure 2.21 – Polycarbonate films ablated under different laser focusing conditions.

## II.2.3 EXPERIMENTAL SETUP

To study the ablation of polycarbonate coated RDX films, the following experimental setup shown in the Figure 2.22 was constructed. The core of the system is a

stainless steel cross with a 15 mm interior diameter. The front port of the chamber is fitted with a UV-grade quartz window to allow laser irradiation of the sample. A 10 x 10 mm sample is attached to a stainless steel stub at the opposite end of the cross from the window with adhesive tape. An MKS Baratron pressure gauge with a working range of 1000 Torr is attached to one of the perpendicular ports (see Figure 2.22) to monitor the pressure in the chamber.  It is connected to an MKS PDR-2C power supply digital readout which is in turn connected to an NB-MIO-16 I/O Board in an Apple Macintosh computer. The system also can be connected to a vacuum pump via the remaining port on the cross by a valve. In this work, laser ablation is conducted at ambient pressure with the valve closed. The pressure (mm Hg) reading data as a function of number of points is collected by means of a Lab View 5.1 interface with the rate of 250 points/s. Laser irradiation is achieved using the fourth harmonic output (266 nm, 4 ns) of a Nd-YAG laser (Continuum Inlite-III-10). Laser fluence at the surface of the sample is controlled by adjusting the distance between the sample and 140 mm focal length lens mounted on an optical rail. An IBM compatible computer is used to control various laser parameters such as flahlamp voltage and frequency, and the Q-switch delay and divider through a serial port connection using hyper terminal. All experiments were conducted with a 190 microsecond Q-switch delay and 1300 V, 10 Hz and the Q-switch divider was used to allow laser pulsing at an integer fractions of the 10 Hz flash lamp frequency. The laser focus was set at 100 mm to insure that multiple laser shots were required to ablate completely through a standard RDX film.  The standard RDX film was prepared by spraying 0.8 mg of RDX solution from a sprayer to sample distance of 80 mm, resulting in a spot that was 5 mm in diameter.                                                                     .
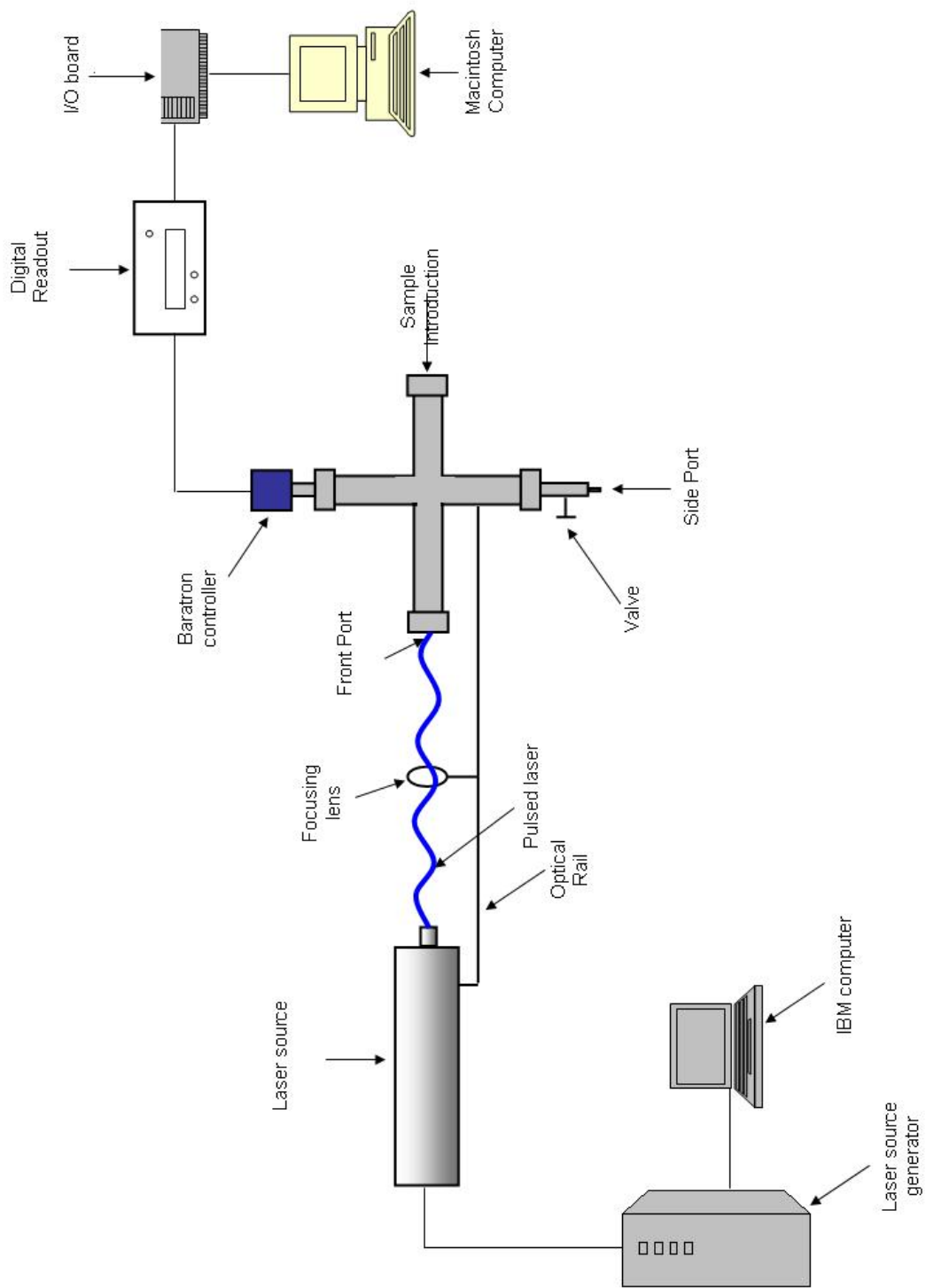
Figure 2.22 – Laser ablation experimental setup.

47

II.2.4 RESULTS AND DISCUSSION

To investigate whether the ablation plasma generated in the polymer film can create a short-lived ignition of the propellant, "sandwich" structures of the polymer on propellant have been prepared, see Figure 2.23 (a).
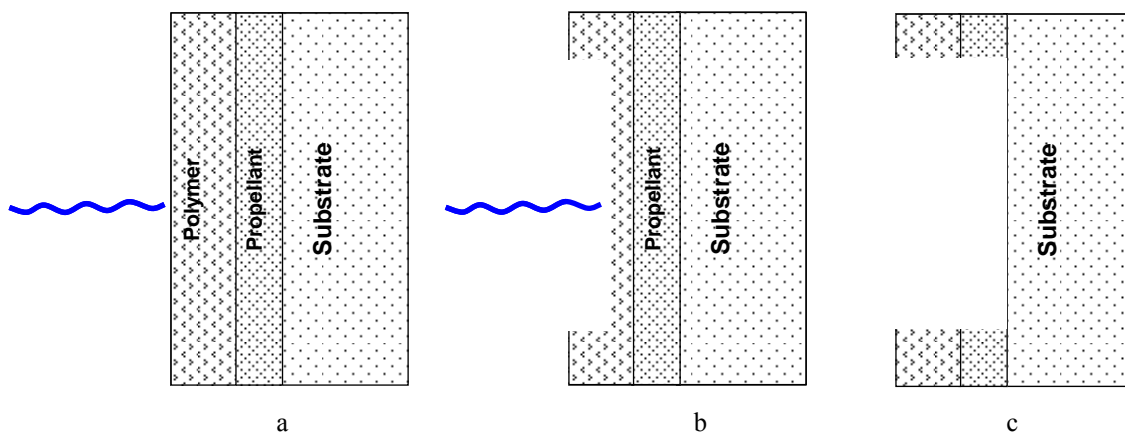


Figure 2.23 – Sandwich structure samples: a) before ablation; b) after 1$^{st}$ shot; c) after 2$^{nd}$ shot

RDX solution was sprayed with a nebulizer on a 10 x 10 mm glass substrate, and a polycarbonate film was spin coated over the propellant film. In Figure 2.23 (b), a schematic illustration of a "sandwich" sample after exposure to a number of laser pulses is shown. Since the valve is closed, a pressure change in the vessel is anticipated with each laser pulse as the polycarbonate film is ablated. The magnitude of the pressure change should be the same as those observed for the ablation of bulk polycarbonate films. After the polycarbonate film has been ablated to a thickness of less than the thickness ablated by a single laser pulse, see Figure 2.23 (c), the following pulse will create a

polycarbonate ablation plasma in contact with the underlying RDX layer. If ignition is achieved, the entire RDX film will erode in a single laser shot and a pressure change larger than that observed for a single laser shot on a pure RDX film will be observed. If ignition is not achieved, multiple laser pulses will be required to ablate through the RDX, and the magnitude of the pressure changes observed for each shot should be the same as that observed for a pure RDX film.
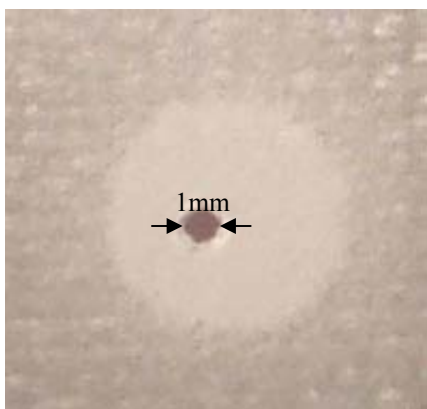


Figure 2.24 – Ablated RDX film sprayed on a glass substrate.

Before the experiments with "sandwich" samples were conducted, pure RDX films as well as polycarbonate films were ablated. The focusing lens to sample distance was chosen such that RDX film ablates in several shots. At a focusing distance of 100 mm, it was found that it takes 3 laser shots to break through the RDX film. The spot formed as a result of ablation is 1 mm in diameter (see Figure 2.24) so that the amount of material removed per each shot is $3.2 \times 10^{-5}$ g.

Figure 2.25 is a plot of the pressure change observed as a 27 micron thick spin coated polycarbonate film is ablated. The ablation was conducted with a frequency of 1 Hz. The expected number of laser pulses to break through the 27 μm thick polycarbonate film is 40 (see calibration curve, Figure 2.20). No pressure rise beyond the noise level is observed. This result may be explained by considering both the amount of polycarbonate ablated and the details of the chemical processes involved in polycarbonate combustion.
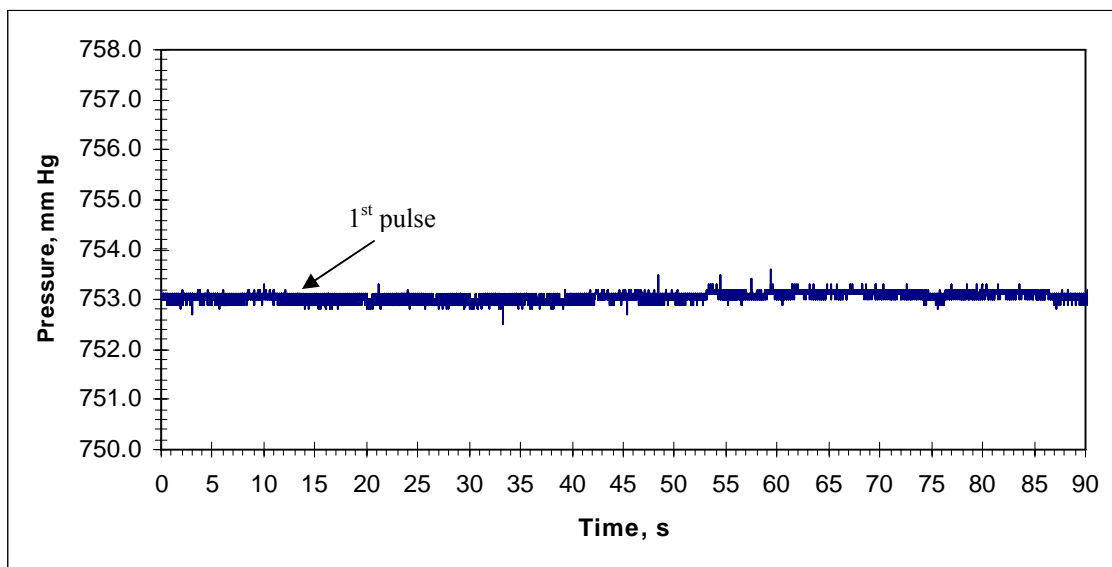
Figure 2.25 – Pressure as a function of time for ablation of polycarbonate film.

At a lens to sample distance of 100 mm a single laser pulse results in a pit that is 500 μm in diameter and 0.64 μm deep, see results in Figures 2.19 and 2.20. The total ablated volume is then $1.25 \times 10^5$ μm$^3$. Using the density of polycarbonate (1.2 g/cm$^3$), a mass of $1.5 \times 10^{-7}$ g or $5.9 \times 10^{-10}$ moles of the monomer are ablated in each laser shot. The complete combustion of polycarbonate is:

$$C_{16}H_{14}O_{3\,(s)} + 18O_{2\,(g)} \longrightarrow 16CO_{2\,(g)} + 7H_2O_{\,(l)} \qquad \text{(i)}$$
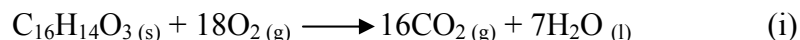
Since the pressure measurement is made on the millisecond timescale, and the air within the vessel is at ambient temperature before and after the ablation event, the water is expected to condense and the only gas product is $CO_2$. In this reaction, more $O_2$ is consumed than $CO_2$ is produced so a net pressure decrease might be expected. Assuming a volume of the vessel (including the Baratron gauge) of approximately $3.96 \times 10^{-5}$ m$^3$, a pressure drop of only $2.73 \times 10^{-4}$ mm Hg would be anticipated, which would not be detectable. In addition, complete combustion is not typically observed in polycarbonate combustion, meaning that CO is anticipated as a product [39] along with the

50

soot deposited around the ablation pits. The balanced reaction for the production of only $CO_{(g)}$ in the combustion of polycarbonate is:

$$C_{16}H_{14}O_{3\ (s)} + 10O_{2\ (g)} \longrightarrow 16CO_{(g)} + 7H_2O_{(l)} \qquad \text{(ii)}$$

This reaction results in a net production of 6 gas molecules and a net increase in pressure that would be three times larger than the loss pressure for the complete combustion, but that would still be below detectable levels. The production of soot, primarily $C_x$, requires no consumption of $O_{2\ (g)}$ and produces no gas products and so is expected to have no influence on the total pressure. Since the actual combustion of the polycarbonate is some combination of the three processes, it does not seem unreasonable to believe that no net pressure increase might be observed even if its magnitude were not below the detection limit of the Baratron gauge used.

Figure 2.26 is a plot of pressure change as an RDX film is ablated. The ablation was conducted with a frequency of 0.2 Hz. The expected number of laser pulses to break
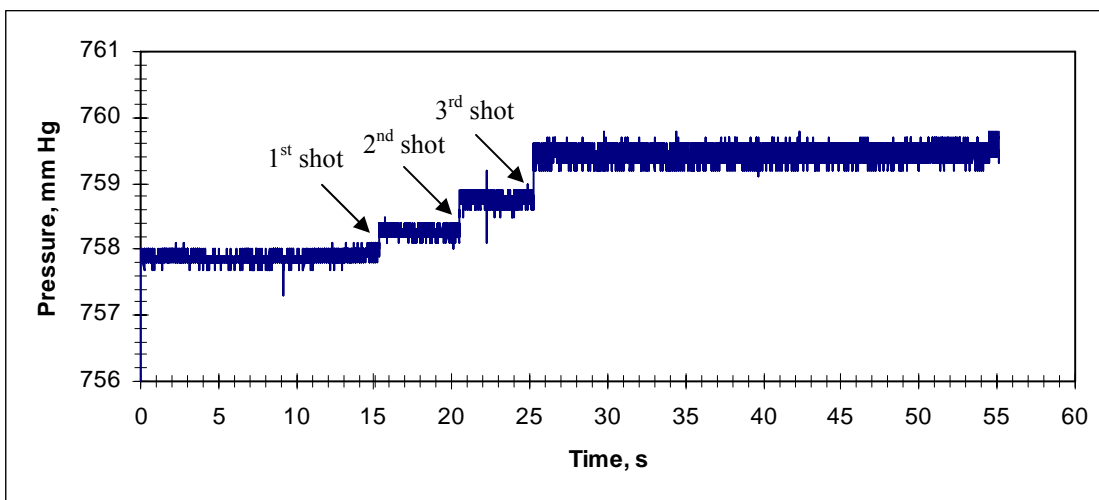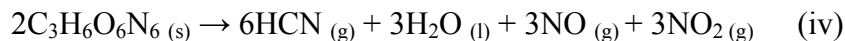


Figure 2.26 – Pressure as a function of time for ablation of RDX film.

through the RDX film is 3. The reaction products of RDX are not well known, but a simple model of the reaction might be expected to result in the net formation of at least 6 molecules by either simple fragmentation (iii) or complete combustion to stable products (iv):

$$C_3H_6O_6N_6 \text{ (s)} \rightarrow 3CH_2N \text{ (g)} + 3NO_2 \text{ (g)} \qquad\qquad \text{(iii)}$$

$$2C_3H_6O_6N_6 \text{ (s)} \rightarrow 6HCN \text{ (g)} + 3H_2O \text{ (l)} + 3NO \text{ (g)} + 3NO_2 \text{ (g)} \quad \text{(iv)}$$

The amount of RDX removed per each shot is $3.2 \times 10^{-5}$ g which makes $1.44 \times 10^{-7}$ moles of RDX. Thus, $8.64 \times 10^{-7}$ total moles of gas formed during combustion. This accounts for a pressure rise of 0.4 mm Hg per each shot. From the Figure 2.23, first two shots each raised the pressure by ~ 0.4 mm Hg which is in close agreement with calculated pressure change. The $3^{rd}$ shot resulted in larger pressure rise of 0.7 mm Hg. The experimental error is $\pm 0.2$ mm Hg.

Figure 2.27 is a plot of pressure change as a polycarbonate coated RDX film is ablated. The ablation was conducted with a frequency of 0.2 Hz. The expected number of
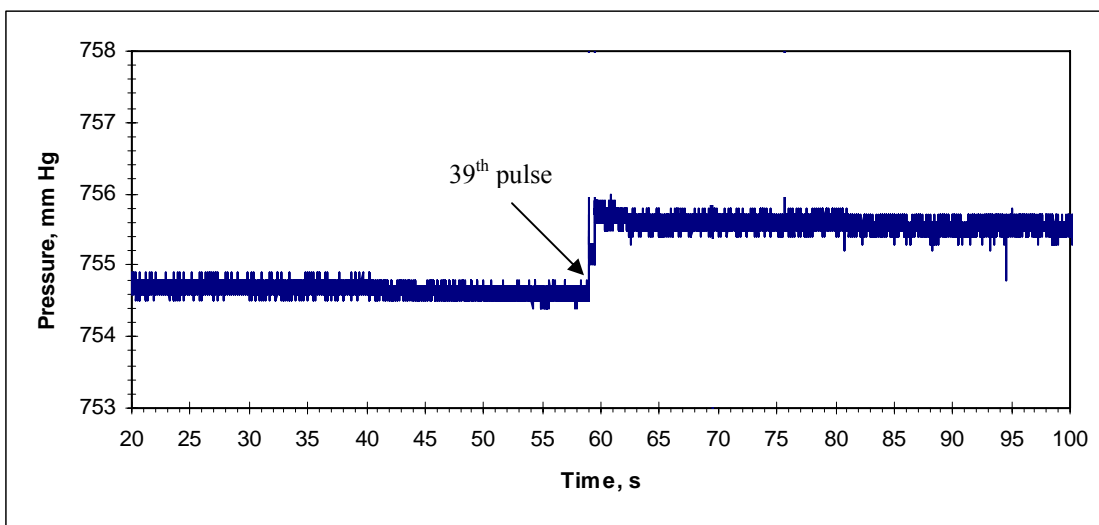


Figure 2.27 – Pressure as a function of time for polymer coated RDX film.

laser pulses to break through the 27 μm thick RDX film is 40. The pressure rise of ~ 1 mm Hg is observed as the 39$^{th}$ laser pulse reaches the underlying RDX film and completely breaks through it. The result is within the experimental error of ± 0.2 mm Hg as compared to calculated total pressure increase of 1.2 mm Hg.

It is not unreasonable to believe that this 39$^{th}$ laser pulse generated a high pressure, high temperature polycarbonate ablation plasma in contact with the underlying RDX film and the entire RDX film has eroded in one shot resulting in ignition. More experiments at various laser ablation conditions need to be done to prove that laser ignition of propellants can be achieved.

# REFERENCES

1. Morris, C. *Academic Press Dictionary of Science and Technology*; Academic Press: New York, 1992; 1829.

2. Cook, Melvin, A. *Science of high explosives*; Reinhold Pub. Corp.: New York, 1958; pp. 2-13.

3. Baily, A. *Explosives, propellants, and pyrotechnics*; Murray, S. G.; Brassey's: London, 1989, pp. 11-15.

4. Woodley, C.R. *IEEE Trans. Mag.* **1993**, 29, 625.

5. Edwards, C.M., Bourham, M.A., Gilligan, J. G. *IEEE Trans. Mag.* **1995**, 31, 404.

6. Pesce - Rodriguez, R.A., Beyer, R.A. *A Theory of Plasma-Propellant Interaction;* ARL-TR-3286.

7. Chaboki, A., Zelenak, S., Isle, B. *IEEE Trans. Mag.* **1997**, 33 (1), 284-288.

8. Haak, H. K., Scaffers, P., Weise, T. H. G. G., Wisken, H.G. *IEEE Trans. Mag.* **1997**, 39 (1), 231-234.

9. Nusca, M. J., McQuaid, M. J. *CPIA Publ.*, **1999,** 691, 143.

10. Zaghloul, Mofreh, R. Murali, S., Krupakar, Gilligan, J. G., Hankins, O. E., Bourham, M. *CPIA Publ.*, **1998**, 680, vol.1, 247.

11. Kinkennon, A., Birk, A., Del Guercio, M., Kaste, P., Lieb, R., Newberry, J., Pesce – Rodrigues, R., Schroeder, M. *CPIA Publ.*, **2000**, 697, 345.

12. Schroeder, M., Pesce - Rodrigues, R. A. *CPIA Publ.*, **2000**, 710, vol.1, 123.

13. Kaste, Kinkennon, P. A., Lieb, R., Birk, A., Del Guercio, M., Newberry, J., Schroeder, M., Pesce - Rodrigues, R. *CPIA Publ.*, **1999**, 691, 77.

14. Andreasson, S., Carlson, M. U. *IEEE Trans. Mag.* **1999**, 35, 181.

15. Katulka, G. L., White, K. J., Oberle, W. F., Kaste, P., Pesce - Rodriguez, R. *IEEE Trans. Mag.***1999**, 35, 197.

16. Pesce - Rodriguez, R. *Current Thinking on Plasma/Propellant Interactions;* Army Plasma/Propellant Interaction Workshop, **2003**.

17. Oberle, W., Wren, G. *IEEE Trans. Mag.* **1999**, 35, 207.

18. Alimi, R., Goldenberg, C., Perelmutter, L., Melnik, D., Zoler, D. *IEEE Trans. Mag.* **1999**, 35, 175.

19. Kappen, K., Baunder, U. H. *IEEE Trans. Mag.* **1999**, 35, 192.

20. Thynell, S. T., Zhou, H., Li, J. Q., Litzinger, T. A. *CPIA Publ.*, 1999, 691, 119.

21. Ngo, H. H., Bourham, M., Doster, J. M. *CPIA Publ.,* **1998**, 680, vol.1, 187.

22. Donnelly, V. M., *J. Vac. Sci. Technol. A.*, **1996**, 14, 3, 1076.

23. Postawa, Z., Czerwinski, B., Szewczyk, M., Smiley, E. J., Winograd, N., Garrison, B., *J. Phys. Chem. B.,* **2004**, 108, 7831.

24. Blumenthal, R. *Interim Report* (W911NF-04-1-0213), 08/2005.

25. Haglund, R. F., Jr. *Laser Ablation and Desorption*; Miller, J. C., Haglund, R. F., Eds.; Academic Press: San Diego, 1998, 15-138.

26. Srinivasan, R., *Science,* **1986**, 234, 559.

27. Srinivasan, R., Braren, B. *Chem. Rev.,* **1989**, 89, 1303.

28. Kim, H., Hambir, S. A., Dlott, D. D. *Phys. Rev. Lett*. **1999**, 83 (24), 5034.

29. Zhigilei, L. V., Garrison, B. J. *Appl. Phys. A*. **1999**, 69, S75.

30. Varghese, P. L., Clemens, N. T. *Interim Report* (DAAD19-00-1-0420), 12/2000.

31. Brodie, I., Murray, J. J. *The Physics of Micro/Nano-Fabrication*; Plenum Press: New York, 1992.

32. Richardson, Tim H. *Functional organic and polymeric materials: molecular functionality-macroscopic reality;* Chichester: New York, 2000, pp. 18-27.

33. Chin, D., Janata, A. *J. Thin Solid Films*. 1994, 252, 145.

34. Scully, M., Petty, M. C., Monkman, A. P. *J. Synth. Met*. **1993**, 183, 55.

35. Critchley, S. M., Willis, M. R, Cook, M. J., McMurdo, J., Maruyama, Y. *J. Mater. Chem.* **1992**, 2, 157.

36. Petty, M., Tsibouklis, J., Petty, M. C., Feast, W. *J. Ferroelectrics.* **1993**, 150, 267.

37. Wu, C.-C., Sturm, J. C., Register, R. A., Tian, J., Dana, E. P., Thompson, M. E. *IEEE Trans. Elec. Dev*. **1997**, 44, 1269.

38. Orland, A., Blumenthal, R. *J. Propulsion Power.* **2005**, 21 (3), 571-573.

39. Hansen, S. G., Robitaille, T. E. *J. Appl. Phys.* **1989**, 66 (3), 1.